WATER RESOURCES RESEARCH, VOL. 49, 2174–2196, doi:10.1002/wrcr.20178, 2013

Semianalytical solutions for release of fluids from rock matrix blocks with different shapes, sizes, and depletion regimes

Ehsan Ranjbar,[1] Hassan Hassanzadeh,[1] and Zhangxin Chen[1]

Received 10 September 2012; revised 7 January 2013; accepted 2 March 2013; published 26 April 2013.

[1] Dual-porosity (DP) models have been extensively used to simulate the flow of fluids (water or gas) in aggregate soils and fractured porous media. The fluid exchange between the rock matrix blocks and the fracture network is very important in DP models. In this study, we present semianalytical solutions for release of a single-phase liquid or gas from cylindrical and spherical matrix blocks with various block size distributions and different pressure depletion regimes in the fracture. The nonlinear pressure diffusivity equations for flow of gas and air are solved analytically using an approximate integral method. It is shown that this solution can be simplified to model flow of slightly compressible fluids like water in DP media. The effect of variable block size distribution on the release rate for different block geometries is studied. Practically it is not feasible to model a large-scale fractured reservoir based on a fine grid approach due to the requirement of large computational time. The presented semianalytical model can be incorporated into numerical models for accurate modeling of the amount of transferred fluid between matrix and fractures using a DP approach. It is shown that the results calculated by the developed model match well with those from fine grid numerical simulations. Furthermore, the developed model can recover the available solutions in the literature for slightly compressible fluids such as water or oil. It can be used to calculate two- or three-dimensional flows in matrix blocks bounded by two or three sets of fractures, respectively.

Citation: Ranjbar, E., H. Hassanzadeh, and Z. Chen (2013), Semianalytical solutions for release of fluids from rock matrix blocks with different shapes, sizes, and depletion regimes, *Water Resour. Res.*, *49*, 2174–2196, doi:10.1002/wrcr.20178.

1. Introduction and Previous Studies

[2] The fluid flow and transport in fractured rocks is of great significance in many groundwater environments [*Novakowski and Lapcevic*, 1994]. Flow and transport in fractured porous media are often described using a dual-porosity (DP) model. This model assumes that the porous medium includes two different regions, one related with the macropore or fracture network with high permeability and the other with a less permeable and more porous system of soil aggregates or rock matrix blocks. DP models assume that both water flow and solute transport can be described by two equations for matrix and fractures, which are coupled using a term describing the exchange of fluid or solutes between the two pore regions [*Gerke and van Genuchten*, 1993]. The DP approach has been used in numerical simulation of groundwater, oil, and gas flow in fractured porous media. However, for large-scale simulations the use of this approach is limited by the huge number of grid-blocks and small time steps that are often needed to accurately simulate the flow and are expensive in terms of computational time. Therefore, developing analytical and semianalytical approaches that can handle fractured porous media or structured soils with less computational time is important [*Zimmerman and Bodvarsson*, 1989].

[3] Study of gas flow in unsaturated soils and fractured porous media is significant in a variety of engineering fields. In agricultural engineering, airflow in the root zone due to barometric pressure variation is important to plant growth. Recent studies have shown that airflow can be applied to create a dry barrier for waste disposal facilities [*Shan*, 1995]. Complex gas-water processes in fracture-matrix systems are the main processes in a range of environmental engineering systems, changing from CO_2 storage in deep geological formations [*Altevogt and Celia*, 2004; *Chen and Zhang*, 2010] over radioactive waste disposal in caverns to evaporation processes in the unsaturated zone [*Nuske et al.*, 2010]. As an example, soil vapor extraction is a widely used technique to eliminate volatile organic contaminants from the unsaturated zone [*Falta*, 1995]. In this process, gas is induced by vapor extraction for cleaning up vadose zone contamination of volatile organic chemicals. The gas flow is also important in the unsteady flow of air in an anisotropic layer of snow [*Fan and Yen*, 1968].

[4] Another important aspect of gas flow in the fractured media is air injection tests to determine the hydrologic properties and parameters of the fracture networks [*Huang et al.*, 1999]. *Illman and Neuman* [2001] developed pressure and

[1]Department of Chemical and Petroleum Engineering, Schulich School of Engineering, University of Calgary, Calgary, Alberta, Canada.

Corresponding author: H. Hassanzadeh, Department of Chemical and Petroleum Engineering, Schulich School of Engineering, University of Calgary, 2500 University Drive NW, Calgary, AB T2N 1N4, Canada. (hhassanz@ucalgary.ca)

0043-1397/13/10.1002/wrcr.20178

pressure derivative type curves for single-phase airflow. *Illman* [2005] analyzed the single-hole pneumatic injection and recovery tests for determining permeability, porosity, and skin. *Shan* [1995] developed analytical solutions for transient, one-dimensional gas flow caused by barometric pumping, and applied these solutions to estimate the air permeability of the vadose zone. In geothermal reservoirs, water and vapor (steam) transport occurs in fractured porous media. There are several studies relevant to flow of fluids in geothermal reservoirs, which is another important application of compressible fluids (vapor) flow in the fractured media [*Pruess*, 1983; *Fitzgerald and Woods*, 1998]. *Schrauf and Evans* [1986] and *Parker et al*., [2006] studied the flow of gas in a single natural fracture and porous media, respectively.

[5] In hydrology, there exist a large number of mathematical models (numerical, analytical, or semianalytical) to simulate the flow of compressible fluids in underground environments and structured soils [*You et al*., 2011]. *McWhorter* [1990] presented an exact semianalytic solution for transient radial gas flow and applied it for estimating the gas permeability using pumping test data. *Wang and Dusseault* [1991] obtained analytical solutions for compressible fluids flowing through a saturated poroelastic medium by solving a new density diffusion equation. *Falta* [1995] developed an analytical solution for transient and steady state compressible gas flow to a pair of horizontal wells in an unsaturated zone. *Shan et al*. [1999] presented analytical solutions for transient, two-dimensional (2-D) gas flow in a vertical vadose (unsaturated) zone section, and presented techniques for approximating the air permeability of a vertical leaky fault. *Shan* [2006] developed an analytical solution for transient gas flow in a multiwell system.

[6] In the case of gas-water displacement, *Thunvik and Braester* [1990] analyzed the displacement of gas-water in fracture networks with different permeability and different inclination by focusing mainly on the gas breakthrough time. *Berger and Braester* [2000] presented a mathematical model for displacement of gas-water in the fracture networks with a nonlinear system of partial differential equations and solved this system numerically using an iterative approach.

[7] Flow of compressible and slightly compressible fluids (water or oil) in fractured reservoirs has been studied extensively with applications in prediction of production rates and well testing [*Warren and Root* 1963; *Kazemi et al*., 1976; *Zimmerman et al*., 1993, 1996; *Civan and Rasmussen*, 2002; *Penuela et al*., 2002; *Bogdanov et al*., 2003; *Lu and Connel*, 2007; *van Heel et al*., 2008; *Mora and Wattenbarger*, 2009; *Hassanzadeh et al*., 2009; *Ranjbar and Hassanzadeh*, 2010; *Ranjbar et al*., 2011; *Mourzenko et al*., 2011; *Ranjbar et al*., 2012; *Ye and Ayala*, 2012]. As an example, *Hoteit and Firoozabadi* [2005] developed a discrete fracture model to simulate the flow of compressible fluids in homogeneous, heterogeneous and fractured porous media.

[8] There are also a number of studies that have considered the effect of block geometries on DP fluid flow formulation [*Barker*, 1985; *van Genuchten and Dalton*, 1986; *Wuthicharn and Zimmerman*, 2011]. As an example, *Zimmerman et al*. [1990] developed a DP model based on an approximate solution for absorption of water into slab-shaped, cylindrical, and spherical blocks.

[9] According to the aforementioned works, the flow of compressible fluids like gases and air in porous media is important in hydrological, environmental, and petroleum engineering. In our previous studies, semianalytical models for a slab-shaped (one-dimensional) matrix block was developed and the effect of fracture pressure depletion regimes and matrix block size distribution was investigated [*Ranjbar and Hassanzadeh*, 2011, *Ranjbar et al*., 2011, 2012].

[10] The main objective of this study is to develop a new semianalytical model for different matrix block geometries (cylindrical and spherical) for flow of compressible and slightly compressible fluids in fractured porous media. It is emphasized that it is not practical to model a large-scale fractured reservoir based on a fine grid approach due to the requirement of large computational time. The presented semianalytical model can be incorporated into numerical models for accurate modeling of the amount of transferred fluids between matrix and fractures using available DP formulation. In other words, this study is important to reduce the computational time for large-scale simulations of gas flow in fractured porous media and can be nested in a numerical model to resolve subgridblock-scale flows.

[11] In the case of compressible fluids, the presented model may find applications for soil vapor extraction, geological CO_2 sequestration, hydrological determination of fracture properties by air injection, and flow of gas in DP reservoirs. For slightly compressible fluids the presented model is capable to model flow of water or oil in fractured media for different block geometries and different block size distributions. In the presented study, the models for release of fluids from cylindrical (representative of two sets of fractures or 2-D) and spherical (representative of three sets of fractures or three-dimensional (3-D)) blocks are derived. The presented models can be expressed explicitly in terms of time and does not require the numerical inversion or infinite series calculations. This solution approach can significantly decrease the computational time of DP models with an acceptable accuracy.

2. Approximate Analytical Solution

[12] A transfer function is utilized to characterize the matrix-fracture interaction and determine the mass transfer between the matrix blocks and the fractures. The rate of mass transferred from the matrix to the fractures is directly related to the shape factor. For modeling of naturally fractured reservoirs, an exact value of the shape factor is required to account for both the transient and pseudo steady-state behavior of the matrix-fracture interaction and also the geometry of the matrix-fracture system [*Ranjbar and Hassanzadeh*, 2011].

[13] In this section, the DP matrix-fracture transfer function for cylindrical and spherical blocks is derived. After that an approximation is used to derive the matrix-fracture fluid transfer for 2-D flow (cylindrical matrix blocks' approximation) or slab-shaped blocks surrounded by two sets of fractures and 3-D flow (spherical matrix blocks' approximation) or slab-shaped blocks surrounded by three sets of fractures. A similar approach has been used in the

literature [*Zimmerman et al*., 1990; *Lim and Aziz*, 1995; *Hassanzadeh and Pooladi-Darvish*, 2006]. To derive the transfer function for DP cylindrical and spherical blocks we use Darcy's law as given by:

$$q_{\mathrm{sc}} = -\frac{k_m A}{\mu B_g}\frac{\mathrm{d}p}{\mathrm{d}r}. \tag{1}$$

[14] In this equation, A is the surface area, r is the distance from the center of the cylinder or sphere, and B_g is the gas formation volume factor (the volume of fluid at underground conditions divided by the volume of fluid at standard surface conditions). The following equations are used to determine the area for cylindrical and spherical blocks, respectively:

$$A_{\mathrm{Cylinder}} = 2\pi r h, \tag{2}$$

$$A_{\mathrm{Sphere}} = 4\pi r^2. \tag{3}$$

[15] Using the definition of a compressible fluid formation volume factor and the surface area of the cylinder we have:

$$\int_{R_m - r'}^{R_m} \frac{\mathrm{d}r}{r} = -\frac{k_m 2\pi h}{T q_{\mathrm{sc}}}\frac{T_{\mathrm{sc}}}{p_{\mathrm{sc}}}\int_{\overline{p}_m}^{p_f}\frac{p}{\mu Z}\mathrm{d}p. \tag{4}$$

[16] In equation (4), r' is a time-dependent radius where the matrix pressure is equal to its average pressure, h is the height of the cylinder and μ and Z are the gas viscosity and compressibility factor, respectively. In gas reservoirs, pseudo-pressure transformation is used to account for the variability of pressure with viscosity and gas compressibility factor. The pseudo-pressure transformation, which is similar to the Kirchhoff transformation [*Tartakovsky et al*., 1999], is given by:

$$\psi = 2\int_{p_b}^{p}\frac{p}{\mu z}\mathrm{d}p. \tag{5}$$

where p_b is a reference or base pressure. Integrating of equation (4) and using the definition of the real gas pseudo-pressure (equation (5)) leads to the following equations for cylindrical and spherical blocks, respectively:

$$q_{\text{sc-Cylindrical}} = \frac{k_m T_{\mathrm{sc}}}{T p_{\mathrm{sc}}}\frac{2\pi h}{\ln\left(\frac{R_m}{R_m - r'_m}\right)}\frac{\overline{\psi}_m - \psi_f}{2}, \tag{6}$$

$$q_{\text{sc-Spherical}} = \frac{k_m T_{\mathrm{sc}}}{T p_{\mathrm{sc}}}\frac{4\pi R_m(R_m - r')}{r'}\frac{\overline{\psi}_m - \psi_f}{2}. \tag{7}$$

[17] The shape factor for conduction of heat through a cylindrical wall or spherical block is defined as follows, respectively [*Holman*, 2010]:

$$S_{\mathrm{Cylinder}} = \frac{2\pi h}{\ln\frac{D_2}{D_1}}, \tag{8}$$

$$S_{\mathrm{Sphere}} = \frac{4\pi r_1 r_2}{(r_2 - r_1)}. \tag{9}$$

where D_1 and D_2 are the diameters of the inner and the outer cylinders with higher and lower temperatures, respectively, and r_2 is the larger sphere radius with lower temperature. Using the same notion for the case of pressure diffusion, the following equations are used to define the pressure diffusion shape factor for cylindrical and spherical blocks, respectively. This parameter is one of the most important parameters in DP modeling of fractured reservoirs. The amount of fluid that is transferred from matrix to fractures is directly proportional to the shape factor:

$$\sigma_{\mathrm{Cylinder}} = \frac{2\pi h}{\ln\left(\frac{R_m}{R_m - r'}\right)V_b}, \tag{10}$$

$$\sigma_{\mathrm{Sphere}} = \frac{4\pi R_m(R_m - r')}{r' V_b}. \tag{11}$$

[18] In the shape factor equation, V_b is the bulk volume of a matrix block. Using the definition of the shape factor (equations (10) and (11)) in equations (6) and (7) leads to the following equation for the transfer function of a cylindrical and spherical block in terms of the shape factor:

$$q_{\mathrm{sc}} = \frac{k_m T_{sc} V_b}{T p_{sc}}\sigma\frac{\overline{\psi}_m - \psi_f}{2}. \tag{12}$$

[19] The equation for fluid transfer in terms of time derivative can be expressed as follows [*Ranjbar and Hassanzadeh*, 2011]:

$$q_{\mathrm{sc}} = -\frac{T_{\mathrm{sc}} V_b}{2p_{\mathrm{sc}}}\frac{\mu c_m \phi_m}{T}\frac{\partial\overline{\psi}_m}{\partial t}. \tag{13}$$

[20] Solving equations (12) and (13) for the shape factor results in the following equation:

$$\sigma = -\frac{\mu c_m \phi_m}{k_m\left(\overline{\psi}_m - \psi_f\right)}\frac{\partial\overline{\psi}_m}{\partial t}. \tag{14}$$

[21] Solution of the diffusivity equation is used in equations (12) and (14) to derive the matrix-fracture fluid transfer and shape factor for compressible or slightly compressible fluids.

[22] The diffusivity equation for flow of compressible fluid for different geometries can be expressed as follows:

$$\frac{1}{r^I}\frac{\partial}{\partial r}\left(r^I\frac{\partial\psi_m}{\partial r}\right) = \frac{\mu c_m \phi_m}{k_m}\frac{\partial\psi_m}{\partial t}, \tag{15}$$

where for a cylindrical block I=1 and for a spherical block I=2. It should be mentioned that equation (15) is a nonlinear partial differential equation (PDE). This nonlinearity is due to the pressure dependence of viscosity and compressibility of the compressible fluids like air or gas. The diffusivity equation for a cylindrical and spherical block in terms of hydraulic diffusivity, η, (ratio of matrix permeability to the product of gas viscosity, matrix compressibility (fluid and rock) and matrix porosity) can be expressed as follows:

$$\eta\frac{\partial}{\partial r}\left(r^I\frac{\partial\psi_m}{\partial r}\right) = r^I\frac{\partial\psi_m}{\partial t}. \tag{16}$$

[23] At the initial condition a pseudopressure in the matrix block can be obtained from the initial pressure. At the center of the cylindrical or spherical matrix block we have no flow boundary condition and at the outer boundary, the pressure is equal to the fracture pressure, which may be a constant or varies with time. Figure 1 is a schematic representation of the problem for a cylindrical block surrounded by fractures. For a spherical block the problem is the same but instead of a cylinder we are dealing with a spherical block. To solve this equation the average hydraulic diffusivity over the matrix-fracture pressure drawdown is defined as follows [*Ranjbar and Hassanzadeh*, 2011]:

$$\overline{\eta} = \frac{1}{p_f - p_i}\int_{p_i}^{p_f} \frac{k_m}{\mu c_m \phi_m}\mathrm{d}p = \frac{k_m}{\phi_m}\frac{1}{p_f - p_i}\int_{p_i}^{p_f} \frac{\mathrm{d}p}{\mu c_m}. \tag{17}$$

[24] To express the diffusivity equation in dimensionless form the following dimensionless variables are defined:

$$\psi_D = \frac{\psi_m - \psi_i}{\psi_f - \psi_i}, \tag{18}$$

$$r_D = \frac{r}{R_m}, \tag{19}$$

$$\eta_D(t) = \frac{\eta_m(t)}{\overline{\eta}}, \tag{20}$$

$$t_D = \frac{\overline{\eta} t}{R_m^2} \tag{21}$$

[25] Using these dimensionless variables in equations (14) and (16) leads to the following equations for the dimensionless shape factor and diffusivity equation:

$$\sigma R_m^2 = -\frac{1}{\eta_D}\left(\frac{1}{\overline{\psi}_D - \psi_{fD}}\right)\frac{\partial \overline{\psi}_D}{\partial t_D}, \tag{22}$$

$$\eta_D(r_D, t_D)\frac{\partial}{\partial r_D}\left(r_D^I \frac{\partial \psi_D}{\partial r_D}\right) = r_D^I \frac{\partial \psi_D}{\partial t_D}. \tag{23}$$

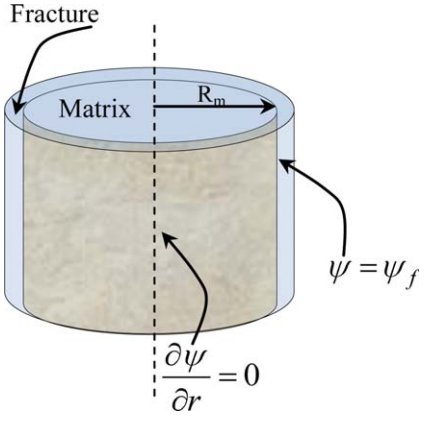

Figure 1. Schematic representation of the problem for a cylindrical block.

[26] In this equation, the hydraulic diffusivity is a function of the dimensionless radius and dimensionless time. For solving this equation we assume that η_D is only a function of the dimensionless time. To consider the effect of the space we multiply η_D by a correction factor β and numerical simulation is used to find this correction factor [*Ranjbar and Hassanzadeh*, 2011]. Therefore, we have the following dimensionless equation for the diffusivity equation of the cylindrical or spherical block:

$$\frac{\partial}{\partial r_D}\left(\beta \eta_D(t_D) r_D^I \frac{\partial \psi_D}{\partial r_D}\right) = r_D^I \frac{\partial \psi_D}{\partial t_D}. \tag{24}$$

[27] In this equation, I=1 is used for the cylindrical block and I=2 is used for the spherical block. This equation is solved for different fracture boundary conditions and different block size distributions to derive the shape factor and matrix-fracture fluid transfer for flow of compressible and slightly compressible fluids in fractured porous media or aggregate and structured soils. It should be mentioned that the presented solution in this study calculates the pressure distribution in the matrix block by assuming fractures as a boundary condition.

2.1. Constant Fracture Pressure

[28] In this case, the fracture pressure at the matrix-fracture interface is a constant and we are dealing with a single block. For the constant fracture pressure, we have the following initial and boundary conditions for the nonlinear diffusivity equation (equation (24)):

$$t_D = 0 \rightarrow \psi_D = 0, \tag{25}$$

$$r_D = 0 \rightarrow \frac{\partial \psi_D}{\partial r_D} = 0, \tag{26}$$

$$r_D = 1 \rightarrow \psi_D = \psi_{fD} = 1. \tag{27}$$

[29] An integral method [*Goodman*, 1964, *Zimmerman and Bodvarsson*, 1989, *Pooladi-Darvish et al*., 1994] and the method of moments [*Ames*, 1965] are used to find the early and late time solutions of this equation. After solving the diffusivity equation and integration over the bulk volume of the cylindrical matrix block we obtain the early and late time average dimensionless pseudopressures as follows:

$$\overline{\psi}_D = \frac{\sqrt{48\beta\eta_{D1} t_D}}{3} \qquad t_D < \frac{1}{48\beta\eta_{D1}}, \tag{28}$$

$$\overline{\psi}_D = 1 - 0.664 e^{\omega_1 t_D} - 0.267 e^{\omega_2 t_D} \qquad t_D \geq \frac{1}{48\beta\eta_{D1}}, \tag{29}$$

where ω_1 and ω_2 are defined as follows for a cylindrical block:

$$\omega_1 = -5.77\beta\eta_{D1} \qquad \omega_2 = -58.23\beta\eta_{D1}. \tag{30}$$

[30] Using the same approach leads to the following early and late time average dimensionless pseudopressures for a spherical block:

$$\overline{\psi}_D = \frac{\delta^3 - 6\delta^2 + 15\delta}{20} \qquad t_D < \frac{17}{720\beta\eta_{D1}}, \tag{31}$$

$$t_D = \frac{3\delta^4 - 16\delta^3 + 30\delta^2}{720\beta\eta_{D1}} \qquad t_D < \frac{17}{720\beta\eta_{D1}}, \tag{32}$$

$$\overline{\psi}_D = 1 - 0.554435e^{\omega_1 t_D} - 0.371074e^{\omega_2 t_D} \qquad t_D \geq \frac{17}{720\beta\eta_{D1}}, \tag{33}$$

where ω_1 and ω_2 for a spherical block are defined as follows:

$$\omega_1 = -9.879736\beta\eta_{D1} \qquad \omega_2 = -76.520264\beta\eta_{D1}. \tag{34}$$

[31] In these equations η_{D1} is the fracture dimensionless hydraulic diffusivity. Derivation of these equations is shown in Appendices A and B in more details. In equation (31), δ is the time-dependent penetration depth for a spherical block and equation (32) is used to relate the penetration depth to the dimensionless time.

[32] Equations (28) and (29) (for a cylindrical block) and (31)–(33) (for a spherical block) and their derivatives with respect to time are substituted into equations (12) and (22) to derive the matrix-fracture transfer rate (release rate) and shape factor for the cylindrical and spherical matrix blocks. To express the rate in the dimensionless form we write Darcy's law over the whole domain of the cylinder to reach the following equation:

$$q_g = \frac{-k_m T_{sc} V_b}{T p_{sc} R_m^2}(\psi_f - \psi_i). \tag{35}$$

[33] Using the definition of the dimensionless pseudopressure in the transfer function (equation (12)) leads to the following equation:

$$q_{sc} = \frac{T_{sc} V_b}{2p_{sc}} \frac{k_m(\psi_f - \psi_i)}{T} \sigma(\overline{\psi}_D - 1). \tag{36}$$

[34] Dividing equation (36) to equation (35) leads to the following equation for the dimensionless release rate for the cylindrical and spherical blocks:

$$q_D = \frac{q_{sc}}{q_g} = -\frac{\sigma R_m^2}{I+1}(\overline{\psi}_D - 1) = \frac{1}{(I+1)\eta_D}\frac{\partial \overline{\psi}_D}{\partial t_D}. \tag{37}$$

[35] Integrating of these equations leads to the dimensionless cumulative fluid release from a cylindrical or spherical block with a constant fracture pressure, respectively:

$$Q_D = \int_0^{t_D} q_D \mathrm{d}t_D = \frac{\overline{\psi}_D}{(I+1)\eta_D}. \tag{38}$$

[36] The early and late time solutions of the diffusivity equation (equations (28) and (29) and (31)–(33)) will be used in equations (37)–(38) to determine the dimensionless rate and the cumulative fluid release for the cylindrical and spherical blocks when the fracture pressure is constant. It should be pointed out that the presented model can be used to model flow of slightly compressible fluids like water or oil if we set $\beta = \eta_{D1} = \eta_D = 1$.

2.2. Variable Fracture Pressure

[37] In this case we assume that the outer boundary condition changes with time. In this section we consider the effect of linearly and exponentially declining fracture pressure on the DP formulation of compressible and slightly compressible fluids.

[38] For the variable fracture pressure the outer time-dependent boundary condition for the diffusivity equation (equation (24)) can be linear or exponential as follows, respectively:

$$\psi_D = \frac{\psi_i - \psi_m}{\psi_i} \rightarrow \psi_{fD}(t_D) = \kappa t_D, \tag{39}$$

$$\psi_D = \frac{\psi_m - \psi_i}{\psi_\infty - \psi_i} \rightarrow \psi_{fD}(t_D) = 1 - \exp(-\kappa t_D). \tag{40}$$

[39] It should be noted that the initial condition and the inner boundary condition are the same as equations (25) and (26), respectively. Using a recently developed semianalytical method to solve the equation for a variable fracture pressure [*Mitchel and Myers*, 2010; *Ranjbar et al*., 2011] we reach the following equations for the average dimensionless pseudopressure for the linearly declining fracture pressure of a cylindrical block:

$$\overline{\psi}_D = \frac{kt_D}{3}\sqrt{16\beta\eta_{D1}t_D}, \qquad t_D < \frac{1}{16\beta\eta_{D1}}, \tag{41}$$

$$\overline{\psi}_D = \kappa t_D - \frac{0.69987\kappa}{\omega_1}(e^{\omega_1 t_D} - 1) - \frac{0.29639\kappa}{\omega_2}(e^{\omega_2 t_D} - 1), \quad t_D \geq \frac{1}{16\beta\eta_{D1}}, \tag{42}$$

where ω_1 and ω_2 are determined based on equation (30) in the case of a cylindrical block. For a spherical block with linearly declining fracture pressure, the following solutions are obtained for the early and late time average dimensionless pseudopressure:

$$\overline{\psi}_D = \frac{\kappa}{260\beta\eta_{D1}}(\delta^5 - 6\delta^4 + 15\delta^3) \qquad t_D < \frac{1}{13\beta\eta_{D1}} \text{ or } \delta < 1, \quad \delta = \sqrt{13\beta\eta_{D1}t_D} \tag{43}$$

$$\overline{\psi}_D = \kappa t_D - \frac{0.626902\kappa}{\omega_1}(e^{\omega_1 t_D} - 1) - \frac{0.359632\kappa}{\omega_2}(e^{\omega_2 t_D} - 1) \quad t_D \geq \frac{1}{13\beta\eta_{D1}}. \tag{44}$$

[40] In the case of an exponentially declining fracture pressure, we have the following equations for the average pseudopressure of a cylindrical block:

$$\overline{\psi}_D = \frac{\sqrt{1 - e^{-\kappa t_D}}}{3} \times \sqrt{24\beta\eta_{D1}t_D\left(2 - \frac{\sqrt{\pi}\,\mathrm{erf}\left(\sqrt{\kappa t_D}\right)}{\sqrt{\kappa t_D}}\right)}, \quad t_D < t^*, \tag{45}$$

$$\overline{\psi}_D = 1 - e^{-\kappa t_D} - 0.58746\left(\frac{1-e^{-\kappa t^*}}{e^{\omega_1 t^*} - e^{-\kappa t^*}}\right)e^{\omega_1 t_D} - 0.07754\left(\frac{1-e^{-\kappa t^*}}{e^{\omega_2 t^*} - e^{-\kappa t^*}}\right)e^{\omega_2 t_D} + \left[0.58746\left(\frac{1-e^{-\kappa t^*}}{e^{\omega_1 t^*} - e^{-\kappa t^*}}\right) + 0.07754\left(\frac{1-e^{-\kappa t^*}}{e^{\omega_2 t^*} - e^{-\kappa t^*}}\right)\right]e^{-\kappa t_D}, \qquad t_D \geq t^*. \tag{46}$$

[41] In the case of a spherical block and exponentially declining fracture pressures, the following equations are obtained for the average dimensionless pseudopressure:

$$\overline{\psi}_D = \frac{1-\exp(-\kappa t_D)}{20}\left(\delta^3 - 6\delta^2 + 15\delta\right) \qquad t_D < t^*$$

$$\delta(t_D) = \sqrt{18\beta\eta_{D1} t_D\left(\frac{2}{1-e^{-\kappa t_D}} - \frac{\sqrt{\pi}}{1-e^{-\kappa t_D}}\frac{\mathrm{erf}\left(\sqrt{\kappa t_D}\right)}{\sqrt{\kappa t_D}}\right)}, \tag{47}$$

$$\overline{\psi}_D = 1 - e^{-\kappa t_D} + 0.439073\left(\frac{1-e^{-\kappa t^*}}{e^{-\kappa t^*} - e^{\omega_1 t^*}}\right)e^{\omega_1 t_D} + 0.060923\left(\frac{1-e^{-\kappa t^*}}{e^{-\kappa t^*} - e^{\omega_2 t^*}}\right)e^{\omega_2 t_D} - \left[0.439073\left(\frac{1-e^{-\kappa t^*}}{e^{-\kappa t^*} - e^{\omega_1 t^*}}\right) + 0.060923\left(\frac{1-e^{-\kappa t^*}}{e^{-\kappa t^*} - e^{\omega_2 t^*}}\right)\right]e^{-\kappa t_D}, \qquad t_D \geq t^*, \tag{48}$$

where erf is the error function and t^* is the time at which the effect of pressure disturbance will reach the matrix boundary. Derivation of these equations is shown in Appendices A and B in more details. To determine the dimensionless rate and the cumulative fluid release for variable fracture pressure the same approach as described in section 2.1 is used. The following equation represents the dimensionless release rate for the variable fracture pressure of a cylindrical and spherical block:

$$q_D = -\frac{\sigma R_m^2}{(I+1)}\left(\overline{\psi}_D - \psi_{fD}(t_D)\right) = \frac{1}{(I+1)\eta_D}\frac{\partial\overline{\psi}_D}{\partial t_D}. \tag{49}$$

[42] These equations are integrated to determine the cumulative release from a cylindrical or spherical block with time-dependent fracture pressure.

$$Q_D = \frac{\overline{\psi}_D}{(I+1)\eta_D}. \tag{50}$$

[43] Equations (41)–(48) are substituted into these equations (equations (49) and (50)) to determine the early and late time dimensionless release rates and the cumulative release of fluids for different fracture pressure depletion regimes.

2.3. Variable Block Size Distribution (Multiple Blocks)

[44] In the case of multiple blocks we substitute the collection of blocks with a single block with an equivalent radius [*Zimmerman and Bodvarsson*, 1995; *Ranjbar et al.*, 2012]. To model flow of fluids in fractured media or aggregate soils with multiple cylindrical or spherical blocks of variable block size distributions the following initial and boundary conditions can be written:

$$\frac{1}{r^I}\frac{\partial}{\partial r}\left(r^I\frac{\partial\psi_m}{\partial r}\right) = \frac{1}{\eta_m}\frac{\partial\psi_m}{\partial t}, \tag{51}$$

$$t = 0 \rightarrow \psi_m = \psi_i, \tag{52}$$

$$r = 0 \rightarrow \frac{\partial\psi_m}{\partial r} = 0, \tag{53}$$

$$r = R_{me} \rightarrow \psi_m = \psi_f. \tag{54}$$

[45] It should be noted that in equation (54), R_{me} is the equivalent cylinder or sphere radius and is a function of block size distribution. The following equations are used to find the equivalent radius for discrete and continuous block size distribution, respectively [*Gwo et al.*, 1998; *Ranjbar et al.*, 2012]:

$$R_{me} = \frac{\sum_{i=1}^{N} N_i R_{mi}}{\sum_{i=1}^{N} N_i} = \frac{1}{N_t}\sum_{i=1}^{N} N_i R_{mi} = \sum_{i=1}^{N}\frac{N_i}{N_t}R_{mi} = \sum_{i=1}^{N} f_i(R_{mi})R_{mi}, \tag{55}$$

$$R_{me} = \int_{R_{m\min}}^{R_{m\max}} R_m f(R_m)\mathrm{d}R_m. \tag{56}$$

[46] In equation (56), $f(R_m)$ is the probability density function (PDF), which is used to represent the probability of the blocks as a function of block sizes. In the case of multiple blocks of variable block size distribution in addition to equations (18) and (20), the following dimensionless variables are defined:

$$r_D = \frac{r}{R_{m\max}}, \tag{57}$$

$$t_D = \frac{\overline{\eta}t}{R_{m\max}^2}, \tag{58}$$

$$R_{De} = \frac{R_{me}}{R_{m\max}}, \tag{59}$$

$$f_D(R_D) = R_{m\max} f(R_m), \tag{60}$$

$$F_h = \frac{R_{m\min}}{R_{m\max}}. \tag{61}$$

[47] For the multiple blocks $R_{m\ \max}$, which is independent of the block size distribution, is used to scale the time and radius. Using equations (18), (20), and (57)–(61) in the diffusivity equation and the shape factor equation (equation (14)) for the variable block size distribution, we reach the

following equations for the diffusivity equation, the equivalent radius and the dimensionless shape factor:

$$\frac{\partial}{\partial r_D}\left(\beta\eta_D(t_D)r_D^I\frac{\partial\psi_D}{\partial r_D}\right)=r_D^I\frac{\partial\psi_D}{\partial t_D}, \tag{62}$$

$$t_D=0\rightarrow\psi_D=0, \tag{63}$$

$$r_D=0\rightarrow\frac{\partial\psi_D}{\partial r_D}=0, \tag{64}$$

$$r_D=R_{De}\rightarrow\psi_D=1, \tag{65}$$

$$R_{De}=\sum_{i=1}^{N}f_i(R_{mi})R_{Di}, \tag{66}$$

$$R_{De}=\int_{F_h}^{1}R_Df_D(R_D)\mathrm{d}R_D, \tag{67}$$

$$\sigma R_{me}^2=-\frac{R_{De}^2}{\eta_D}\left(\frac{1}{\overline{\psi}_D-1}\right)\frac{\partial\overline{\psi}_D}{\partial t_D}. \tag{68}$$

[48] To solve the diffusivity equation of multiple cylindrical blocks, the integral method and method of moments are used to find the solution [*Ranjbar et al.*, 2012]. The following equations give the early and late time average dimensionless pseudopressure for multiple cylindrical blocks with block size distribution:

$$\overline{\psi}_D=\frac{\sqrt{48\beta\eta_{D1}t_D}}{3R_{De}}\qquad t_D<\frac{R_{De}^2}{48\beta\eta_{D1}}, \tag{69}$$

$$\overline{\psi}_D=1-0.664e^{\omega_1t_D}-0.267e^{\omega_2t_D}\qquad t_D\geq\frac{R_{De}^2}{48\beta\eta_{D1}}, \tag{70}$$

where ω_1 and ω_2 are defined as follows:

$$\omega_1=\frac{-5.77\beta\eta_{D1}}{R_{De}^2}\qquad\omega_2=\frac{-58.23\beta\eta_{D1}}{R_{De}^2}. \tag{71}$$

[49] Derivation of these equations is shown in Appendix A in more details.

[50] The following equations give the early and late time average dimensionless pseudopressure for multiple spherical blocks with block size distribution using the integral method and method of moments:

$$\begin{aligned}\overline{\psi}_D&=\frac{\delta^3-6R_{De}\delta^2+15R_{De}^2\delta}{20R_{De}^3}\qquad t_D<\frac{17R_{De}^2}{720\beta\eta_{D1}}\\ t_D&=\frac{3\delta^4-16R_{De}\delta^3+30R_{De}^2\delta^2}{720\beta\eta_{D1}R_{De}^2},\end{aligned} \tag{72}$$

$$\overline{\psi}_D=1-0.554435e^{\omega_1t_D}-0.371074e^{\omega_2t_D}\qquad t_D\geq\frac{17R_{De}^2}{720\beta\eta_{D1}}, \tag{73}$$

where ω_1 and ω_2 are defined as follows:

$$\omega_1=\frac{-9.879736\beta\eta_{D1}}{R_{De}^2}\qquad\omega_2=\frac{-76.520264\beta\eta_{D1}}{R_{De}^2}. \tag{74}$$

[51] Derivation of these equations is shown in Appendix B in more details. Table 1 shows the equivalent radius and the PDF for different continuous block size distributions. For the case of discrete block size distribution equation

Table 1. Different Probability Distribution Function and Their Equivalent Radius

Distribution	Distribution Function	Equivalent Radius
Exponential	$f_D(R_D)=\dfrac{ae^{-aR_D}}{e^{-aF_h}-e^{-a}}$	$R_{De}=\dfrac{(aF_h+1)e^{-aF_h}-(a+1)e^{-a}}{a(e^{-aF_h}-e^{-a})}$
Normal	$f_D(R_D)=\dfrac{1}{\sqrt{2\pi\sigma^2}}e^{\left[\frac{-1}{2\sigma^2}(R_D-M)^2\right]}$	$R_{De}=\dfrac{1}{2}\left[\begin{array}{l}M\left[\mathrm{erf}\left(\dfrac{M-F_h}{\sqrt{2\sigma^2}}\right)-\mathrm{erf}\left(\dfrac{M-1}{\sqrt{2\sigma^2}}\right)\right]+\\ \sqrt{\dfrac{2\sigma^2}{\pi}}\left[e^{-\frac{(M-F_h)^2}{2\sigma^2}}-e^{-\frac{(M-1)^2}{2\sigma^2}}\right]\end{array}\right]$
Linear	$f_D(R_D)=mR_D+b$	$R_{De}=\dfrac{m}{3}(1-F_h^3)+\dfrac{b}{2}(1-F_h^2)$
Log-normal	$f_D(R_D)=\dfrac{1}{R_D\sqrt{2\pi\sigma_{\ln}^2}}e^{-\frac{\left[\ln(R_D)-M_{\ln}\right]^2}{2\sigma_{\ln}^2}}$	$R_{De}=\dfrac{e^{M_{\ln}+\frac{\sigma_{\ln}^2}{2}}}{2}\left[\begin{array}{l}\mathrm{erf}\left[\dfrac{M_{\ln}+\sigma_{\ln}^2-\ln(F_h)}{\sqrt{2\sigma_{\ln}^2}}\right]-\\ \mathrm{erf}\left[\dfrac{M_{\ln}+\sigma_{\ln}^2}{\sqrt{2\sigma_{\ln}^2}}\right]\end{array}\right]$

(66) is used to find the equivalent length. More details about these distributions and the corresponding equivalent radius are discussed in *Ranjbar et al*., [2012].

[52] For the case of variable block size distribution, the following equation is used to determine the release rate for the total volume of the reservoir:

$$q_{sc\,R} = \frac{T_{sc}\,V_b}{2p_{sc}}\frac{k_m(\psi_f - \psi_i)}{T}\sigma(\overline{\psi}_D - 1)\frac{R_{mR}}{R_{me}}. \tag{75}$$

[53] In this equation, R_{mR} is the total radius of the reservoir. To determine the dimensionless rate equation (75) is divided by Darcy's rate, which is expressed as follows:

$$q_{g\max} = -\frac{(I+1)}{2}\frac{k_m V_b T_{sc}}{p_{sc}\,TR_{m\max}R_{me}}(\psi_f - \psi_i). \tag{76}$$

[54] The following equations are used to determine the dimensionless rate of release and the dimensionless cumulative release for the variable block size distribution for a cylindrical or spherical block:

$$q_D = -\frac{\sigma R_{me}^2}{(I+1)}(\overline{\psi}_D - 1)\frac{\chi}{R_{De}^2} = \frac{\chi}{(I+1)\eta_D}\frac{\partial\overline{\psi}_D}{\partial t_D}, \tag{77}$$

$$Q_D = \frac{\chi}{(I+1)\eta_D}\overline{\psi}_D. \tag{78}$$

[55] It should be mentioned that in these two equations χ is the ratio of the reservoir radius to the radius of the maximum block. In the result section, we assume that this ratio is 10. The average pseudopressures (equations (69)–(74)) and their derivatives are replaced in equations (77) and (78) to determine the dimensionless rate of release and the dimensionless cumulative release for cylindrical blocks with variable block size distribution. The equations derived for the cylindrical (spherical) block can be used for the 2-D (3-D) flow in the slab-shaped block if the two types of blocks have the same volume. For example, if we set $R_m^2 = h_m^2/\pi$ ($R_m^3 = (3h_m^3)/(4\pi)$) in these equations the solution can be applied for 2-D (3-D) blocks.

3. Model Verification

[56] To determine the validity of the presented model, we compare our results with the fine grid numerical simulation. Cumulative release of fluids from matrix to fractures is used to evaluate the accuracy of the presented model. In addition, comparison of the presented model with models available in the literature for slightly compressible fluids will be used to validate the developed model.

[57] To show the accuracy of the results in the case of 2-D and 3-D flow (two and three sets of fractures) the obtained solution for the average pseudopressure is used in the transfer function equation (equation (12)). Changing all the variables into the dimensional form and integrating this equation over time the following equation is obtained for the cumulative release of fluids for two and three sets of fractures, respectively:

$$Q(t) = \frac{k_m V_b T_{sc}(\psi_i - \psi_f)\pi}{2p_{sc}\,Th_m^2\eta_D}\left\{\begin{array}{ll}\dfrac{h_m\sqrt{48\beta\eta_{D1}}}{3\sqrt{\pi\overline{\eta}}}\sqrt{t} & t < \dfrac{h_m^2}{48\beta\eta_{D1}\pi\overline{\eta}} \\ \dfrac{h_m^2}{\pi\overline{\eta}}\left[1 - 0.664e^{\frac{-5.77\beta\eta_{D1}\pi\overline{\eta}}{h_m^2}t} - 0.267e^{\frac{-58.23\beta\eta_{D1}\pi\overline{\eta}}{h_m^2}t}\right] & t \geq \dfrac{h_m^2}{48\beta\eta_{D1}\pi\overline{\eta}}\end{array}\right\}, \tag{79}$$

$$Q(t) = \frac{k_m T_{sc} V_b(\psi_i - \psi_f)}{2p_{sc}\,T\overline{\eta}\eta_D}\left\{\begin{array}{ll}\dfrac{\delta^3 - 6\delta^2 + 15\delta}{20} & t < \dfrac{17\times 0.384h_m^2}{720\beta\eta_{D1}\overline{\eta}} \\ 1 - 0.554435e^{\omega_1\frac{\overline{\eta}t}{0.384h_m^2}} - 0.371074e^{\omega_2\frac{\overline{\eta}t}{0.384h_m^2}} & t \geq \dfrac{17\times 0.384h_m^2}{720\beta\eta_{D1}\overline{\eta}}\end{array}\right\} \tag{80}$$

$$t = \frac{0.384h_m^2(3\delta^4 - 16\delta^3 + 30\delta^2)}{720\beta\eta_{D1}\overline{\eta}}.$$

[58] It should be pointed out that equations (79) and (80) are obtained from the cylindrical and spherical blocks models with the assumption of having the same volume with blocks formed by two and three sets of fractures, respectively. For example, in the case of a 3-D block (a matrix block formed by three sets of fractures) it is assumed that the sphere and the cube have the same volume [*Lim and Aziz*, 1995].

[59] Figures 2 and 3 compare the cumulative release of gas based on the presented semianalytical model (equations (79) and (80)) and the numerical results (Eclipse 100) for 2-D and 3-D flow, respectively. Based on these figures, the presented semianalytical model is in a good agreement with the fine grid numerical simulations.

[60] Table 2 shows the data that have been used in the fine grid numerical simulations and the presented semianalytical

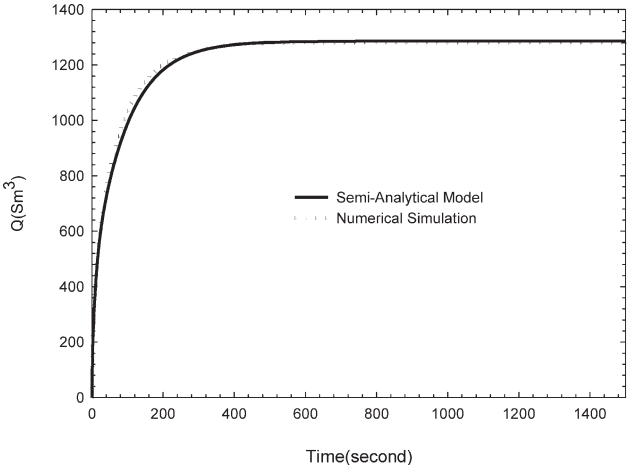

Figure 2. Comparison of the presented model with the numerical simulation for 2-D flow (cylindrical block approximation).

model. It should be mentioned that the data for the semianalytical model and the matching parameters (β and η_D) are the same as those in our previous studies [*Ranjbar and Hassanzadeh*, 2011; *Ranjbar et al*., 2012]. This shows that these parameters are not matrix block geometry dependent.

[61] The presented semianalytical model can recover the shape factors reported in the literature for slightly compressible fluids. Table 3 shows the stabilized values of the shape factor based on this study and the literature models [*Lim and Aziz*, 1995; *Hassanzadeh and Pooladi-Darvish*, 2006] for different boundary conditions and different sets of fractures (2-D and 3-D). As illustrated in this table, there is an acceptable accuracy between the stabilized values of the shape factor based on the presented semianalytical model ($\beta = \eta_{D1} = \eta_D = 1$) and the literature models.

4. Results

[62] In the following the effect of fracture pressure depletion regimes, block size distribution and geometry are studied, respectively.

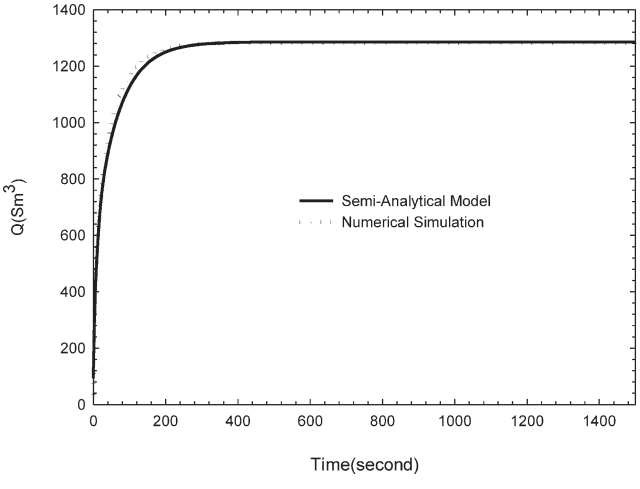

Figure 3. Comparison of the presented model with the numerical simulation for 3-D flow (spherical block approximation).

4.1. Effect of Fracture Pressure Depletion Regime

[63] Three different depletion regimes in the fracture are considered including constant fracture pressure, linear and exponential decline. Results of this study show that the fracture pressure depletion regime will affect the rate of release. In fast depletion regimes like constant fracture and large exponent exponential decline, the matrix depletes more rapidly than that in the case of the linear decline and the small exponent exponential decline.

[64] Figure 4 compares the dimensionless release rate versus the dimensionless time for different depletion regimes in the fracture for a cylindrical block. In the depletion regime of exponential decline with a small exponent, the dimensionless gas release rate is proportional to the square root of the time at the early time. At the middle time, the rate stabilizes to a constant value. The rate eventually drops to zero at the late time. The gas release rate for linearly declining fracture pressure also has the same behavior as the exponentially declining fracture pressure with a small exponent at the early and middle times. For the linear decline, since the decline time is limited to $t_D < 1/k$, the pressure decline in the fracture is not complete and the release rate does not fall to zero.

[65] For the linear decline, the rate of depletion of the matrix increases as the decline rate (k) increases. As illustrated in Figure 4 for the exponential decline, as the value of the exponent increases, the early time release rate increases and the blocks are depleted more quickly. The exponential decline with a large exponent and constant fracture depletion regimes behave in the same way and the block is depleted faster than other depletion regimes. For the fast depletion regimes (constant fracture pressure and exponential decline with a large exponent), the early time dimensionless rate varies inversely proportionally to the square root of the time. A similar observation has been reported for the shape factor in the case of slightly compressible and compressible fluids [*Hassanzadeh and Pooladi-Darvish*, 2006; *Ranjbar et al*., 2011].

[66] It should be mentioned that due to the approximate nature of the presented solution there is a discontinuity in the flux especially for the exponential decline with a large exponent. This discontinuity occurs at t^* where the early and late time solutions coincide. This discontinuity is mainly due to the change in the slope of the pressure (at t^* the early and late time pressures are equal but there is a little difference in their derivatives because of the approximate nature of the solution). Similar behavior is reported by *Zimmerman et al*. [1990] using the integral approximate solutions.

[67] Figures 5 and 6 compare the dimensionless cumulative gas release for different fracture pressure depletion regimes for cylindrical and spherical blocks, respectively. The results show that the time required for the cumulative gas release from a matrix block to reach its plateau depends on the depletion regime in the fracture. Fast depletion regimes like constant fracture pressure and exponential decline with a large exponent reach their plateau more rapidly than those with the linear decline and the exponential decline with a small exponent. On the other hand, the exponential decline with a small exponent and linear decline demonstrate a prolonged release period as compared to the other declines.

Table 2. Data Used for Semianalytical and Numerical Models

Data for fine-grid model
Grid dimension: 28 (22 grids for matrix and 6 grids for fracture)×28 ×1
Grid spacing:
Δx(m): ***1000,20,5***,0.005,0.01,0.15,0.2,0.25,0.3,0.395,0.5,0.5,0.395,0.3,0.25,0.2,0.15,0.01,0.005,***5,20,1000***
Δy: The same as Δx
$\Delta z = 4$ m (for 2-D), for 3-D simulation case the same grid spacing as Δx is used in z-direction.
Fracture porosity = 1
Fracture permeability = 4000 mD
Common data for semianalytical and numerical models
Gas specific gravity = 0.7
Matrix permeability = 1 mD = 9.869233×10^{-16} m^2
Matrix porosity = 0.1
Initial pressure = 45 MPa
Fracture pressure = 22.5 MPa
Reservoir temperature = 366.45 K
$h_m = 4$ m
Data for semianalytical model
B =0.73 p_{sc}=101.325 kPa
η_D=0.3327 T_{sc}=288.7K
η_{DI}=0.3691
$\overline{\eta} = 0.03457$

Table 3. Stabilized Values of the Shape Factor Based on This Study and Literature Models

	Hassanzadeh and Pooladi-Darvish [2006]	*Lim and Aziz* [1995]	*This Study*
2-D flow (cylindrical approximation)			
Constant fracture pressure	18.2	18.17	18.13
Linear decline	25.5		24.86
Exponential decline (small exponent)	25.13		24.84
Exponential decline (large exponent)	18.2		18.13
3-D flow (spherical approximation)			
Constant fracture pressure	25.65	25.67	25.73
Linear decline	39		38.21
Exponential decline (small exponent)	39		37.04
Exponential decline (large exponent)	25.65		25.73

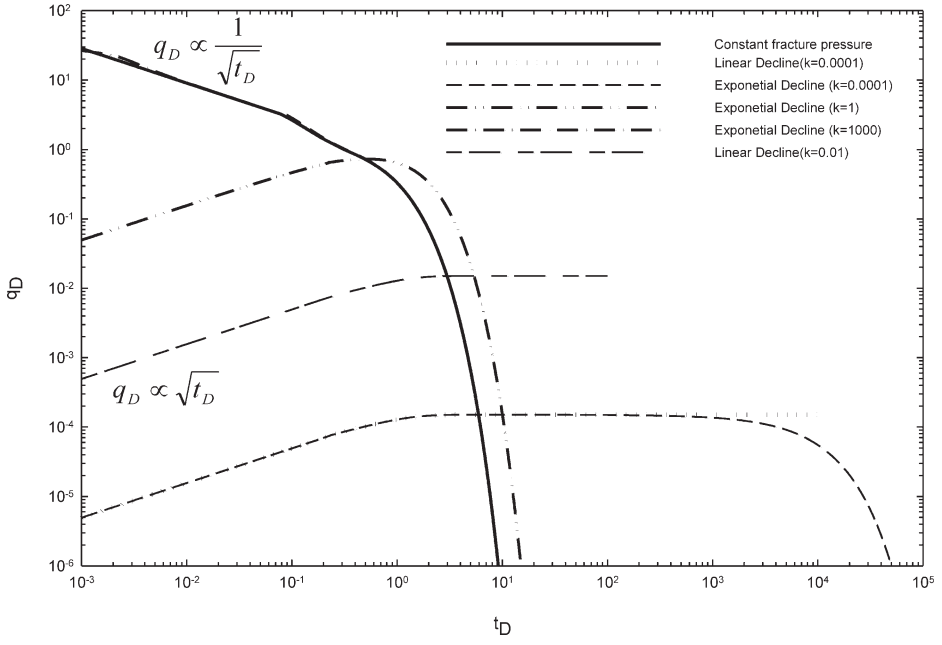

Figure 4. Dimensionless rate versus dimensionless time for different fracture depletion regimes for a cylindrical block.

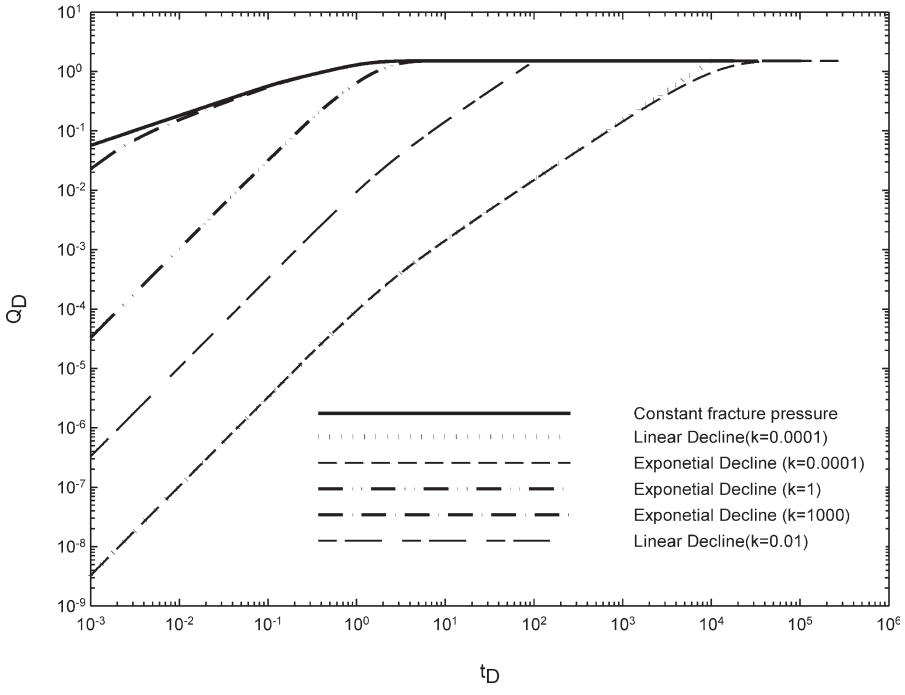

Figure 5. Dimensionless cumulative release versus dimensionless time for different fracture depletion regimes for a cylindrical block.

4.2. Block Size Distribution Effect

[68] In this section, the effect of different block size distribution on the cumulative gas release is investigated. Table 4 illustrates the values of the equivalent radius for different block size distribution. Equations (66) and (67) and Table 1 are used to determine the values of the equivalent radius for different distributions. More details about the distribution and the different values in each distribution are discussed elsewhere [*Ranjbar et al*., 2012]. It should be mentioned that the presented model can also be used for discrete block size distribution as used in our previous study [*Ranjbar et al*., 2012].

[69] Figures 7 and 8 compare the cumulative release for different distributions with cylindrical and spherical blocks,

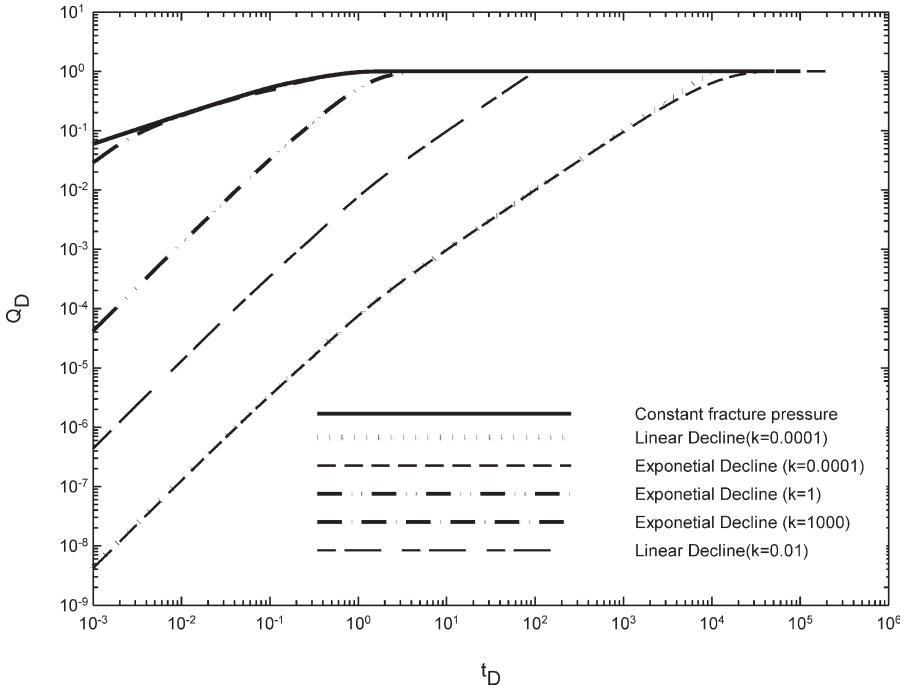

Figure 6. Dimensionless cumulative release versus dimensionless time for different fracture depletion regimes for a spherical block.

Table 4. Values of Dimensionless Equivalent Radius for Different Matrix Block Size Distributions

Block Size Distribution	Dimensionless Equivalent Radius (R_{De})
Ideal distribution	1.000
Exponential distribution (a=−20)	0.950
Linear increasing distribution	0.625
Normal distribution	0.548
Linear decreasing distribution	0.475
Log-normal distribution	0.414
Exponential distribution (a=20)	0.150

respectively. As demonstrated in these figures the time to reach the ultimate cumulative release is proportional to the equivalent radius of the distribution. Based on these figures the exponential distribution with a large exponent is depleted faster than the other distributions. The ideal distribution and exponential distribution with a small exponent behave similarly and deplete more gradually than other distributions.

4.3. Comparison of Different Block Geometries

[70] In this section, we compare the cumulative release for a slab-shaped matrix block with the half thickness of α, a cylinder and a sphere with the radius of α. For the slab-shaped block, the following equation is derived to calculate the cumulative release:

$$Q_D = \frac{1}{\eta_D}\overline{\psi}_D. \tag{81}$$

[71] In our previous study [*Ranjbar and Hassanzadeh*, 2011], the following equations were derived for early and late time average pseudopressure in a slab-shaped matrix block:

$$\overline{\psi}_D = \frac{\sqrt{24\beta\eta_{D1}t_D}}{4} \qquad t_D < \frac{1}{24\beta\eta_{D1}}, \tag{82}$$

$$\overline{\psi}_D = 1 - 0.790e^{-2.486\beta\eta_{D1}t_D} - 0.148e^{-32.181\beta\eta_{D1}t_D} \qquad t_D \geq \frac{1}{24\beta\eta_{D1}}. \tag{83}$$

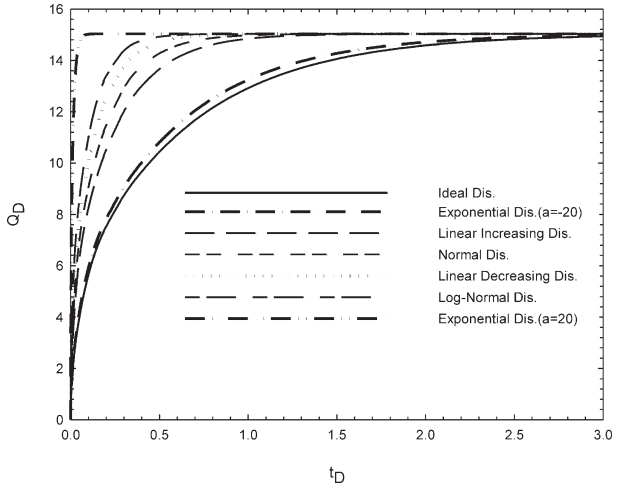

Figure 7. Dimensionless cumulative release versus dimensionless time for different block size distribution and cylindrical blocks.

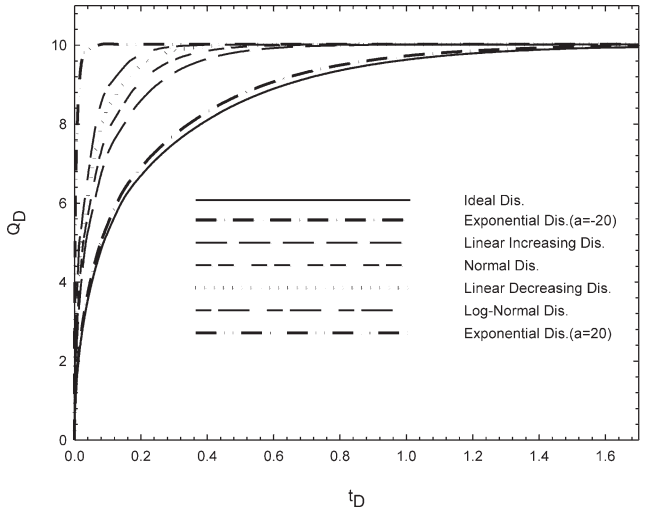

Figure 8. Dimensionless cumulative release versus dimensionless time for different block size distribution and spherical blocks.

[72] Equations (82) and (83) are substituted into equation (81) to determine the cumulative fluid release. For the cylindrical and the spherical block equation (38) (I=1 for cylinder and I=2 for sphere) is derived to determine the cumulative release.

[73] Comparison is performed for different matrix block geometries with the same characteristic length available for release of fluid. Figure 9 compares the dimensionless cumulative release for different matrix block geometries when the fracture pressure is constant. As illustrated in this figure the slab-shaped block has the maximum value of the cumulative release and the blocks are depleted more slowly than the cylindrical and spherical blocks. The spherical block is depleted faster with the smallest value of the final cumulative release. It should be mentioned that using the same characteristic length available for release for different geometries results in blocks with different volumes to the surface area ratio (i.e., $(V/A)_{slab}=2(V/A)_{cylinder}=3(V/A)_{sphere}$).

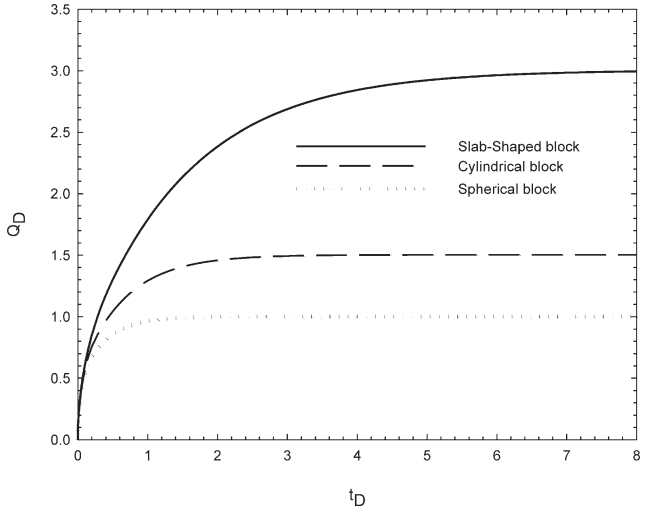

Figure 9. Dimensionless cumulative release versus dimensionless time for different block geometries.

Therefore, the difference observed in the ultimate cumulative release shown in Figure 9 can be explained based on the ratio of the block volume to the block surface area for different geometries with the same characteristic length. It should be noted that in Figure 9 the dimensionless time is scaled based on characteristic length (L_c for slab and R_m for cylinder and sphere). Therefore, different geometries should have the same characteristic length, which results in different ratios of V/A.

[74] Figure 9 shows that the stabilized values of the dimensionless cumulative release are 3.00, 1.50, and 1.00 for the slab-shaped, the cylindrical, and the spherical blocks, respectively. These values can be explained based on the ratio of the volume to the surface area of the blocks for different geometries. The ratio of the volume to the surface area for the slab-shaped block is α, for the cylindrical block it is $\alpha/2$ and for the spherical block it is $\alpha/3$ [*Zimmerman et al.*, 1990]. Therefore, the ultimate cumulative release is proportional to the ratio of the volume to the surface area for different geometries (Assuming the same characteristic length, α, for different geometries). For example, the ratio of (V/A) of the slab to the ratio of (V/A) of the cylinder is two and the ultimate cumulative release for the slab is two times greater than that for the cylinder.

[75] To normalize the cumulative release for three different geometries we scale the dimensionless time by $\tau = \overline{\eta}t/(V/A)^2$and express the normalized cumulative release ($Q(t_D)/Q_{Dt}$) versus the square root of the scaled time (τ) [*Zimmerman et al.*, 1990] where Q_{Dt} is the ultimate cumulative release for any geometry. As an example, the time scale for a sphere of radius α is defined as follows:

$$\tau = \frac{\overline{\eta}t}{(\alpha/3)^2} = 9\frac{\overline{\eta}t}{\alpha^2} = 9t_D. \tag{84}$$

[76] Using the same approach we obtain $\tau = 4t_D$ and $\tau = t_D$ for the cylindrical and slab-shaped matrix blocks, respectively.

[77] Figure 10 demonstrates the normalized cumulative release versus the square root of the scaled time. As a result of the scaling, the release curves become closer to each other for different geometries as illustrated in Figure 10. A similar observation has been made by *Zimmerman et al.* [1990] for absorption curves for different geometries. This scaling law may find applications for irregular shaped blocks, which is beyond the scope of this study.

5. Conclusions

[78] An integral approximation method has been used to derive the solutions for nonlinear pressure diffusion in blocks with different geometries including cylindrical and spherical blocks. The presented solutions have considered the effect of fracture pressure depletion regimes and the variable block size distributions or multiple blocks. The results calculated by the approximate solutions are in good agreement with those calculated by the fine grid numerical models.

[79] It has been shown that the depletion time of a matrix block is a function of the fracture pressure depletion regimes. In the case of constant fracture pressure or exponential decline with a large exponent the block is depleted faster than that in the linear decline and the exponentially decline with a small exponent. For the linear decline and exponential decline with a small exponent the early time dimensionless release rate increases proportionally to the square root of the dimensionless time, then stabilizes at a constant rate and finally falls to zero.

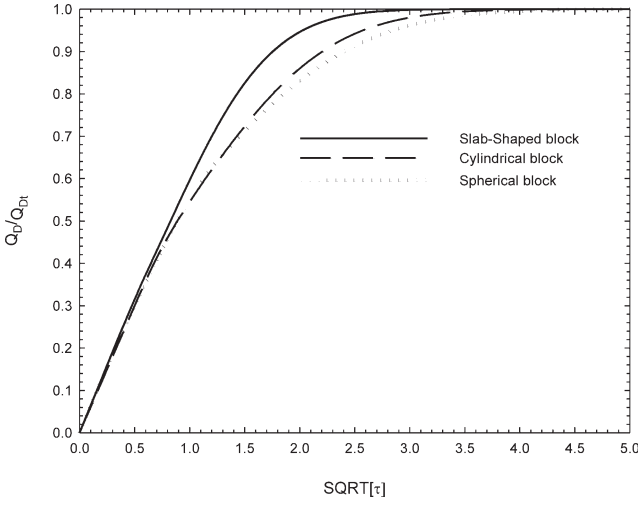

Figure 10. Normalized cumulative fluid release versus square root of scaled time.

[80] Block size distribution is another important parameter that affects the matrix production during the transient state. The blocks with a smaller equivalent radius are depleted more quickly. For a large equivalent radius, distributions like ideal and exponential with a small exponent (i.e., $a=-20$) the transient period is longer than that for the other distributions. Finally, the normalized cumulative release from all matrix block geometries is expressed as a function of the square root of the scaled dimensionless time, which may find application for irregular shape matrix blocks.

Appendix A: Analytical Solution for Cylindrical Blocks

[81] In this Appendix, the solution of nonlinear gas pressure diffusion in a cylindrical matrix block is discussed in more details.

A1. Constant Fracture Pressure

[82] In this case as mentioned in the text the diffusivity equation and its conditions are based on equations (24) (with I=1), (25), (26), and (27).

[83] The integral method is used to find the early time solution by defining the time-dependent penetration depth, $\delta(t_D)$, in which the pressure disturbance has reached that depth. For the early time solution we have the following boundary conditions:

$$r_D = 1 \rightarrow \psi_D = 1, \tag{A1}$$

$$r_D = 1 - \delta(t_D) \rightarrow \psi_D = 0, \quad \frac{\partial \psi_D}{\partial r_D} = 0. \tag{A2}$$

[84] Since the exact solution for the cylindrical block is in the form of first kind, the order zero of Bessel's function

($J_0(r_D)$) we suggest the following polynomial trial solution in the integral method [*Pooladi-Darvish et al*., 1994]:

$$\psi_D = A(t_D) - B(t_D)r_D^2 + C(t_D)r_D^4. \tag{A3}$$

[85] Using actual and auxiliary boundary conditions in the trial solution leads to the following equation:

$$\psi_D = \frac{\left[r_D^2 - (1-\delta)^2\right]^2}{\left[1-(1-\delta)^2\right]^2}. \tag{A4}$$

[86] Using this trial solution in the integral form of the diffusivity equation (equation (24), with I=1) leads to the following solution for early time pseudopressure:

$$\psi_D = \frac{\left[r_D^2 - 1 + \sqrt{48\beta\eta_{D1}t_D}\right]^2}{48\beta\eta_{D1}t_D} \qquad t_D < \frac{1}{48\beta\eta_{D1}}. \tag{A5}$$

[87] It should be noted that η_{D1} is the dimensionless hydraulic diffusivity of the fracture at the outer boundary, which is defined as follows:

$$\eta_{D1} = \eta_D @ x_D = 1 \quad \eta_{D1} = \frac{\eta(x_D=1)}{\overline{\eta}} = \frac{1}{\overline{\eta}}\frac{k}{\mu_f c_f \phi}. \tag{A6}$$

[88] Integrating over the bulk volume of the cylindrical block is used to find the average dimensionless pseudopressure as follows:

$$\overline{\psi}_D = \frac{1}{V}\int_V \psi_D \mathrm{d}V = 2\int_0^1 r_D\psi_D \mathrm{d}r_D. \tag{A7}$$

Substituting equation (A5) into equation (A7) leads to the following equation for the early time average dimensionless pseudo pressure for the cylindrical block in the case of constant fracture pressure:

$$\overline{\psi}_D = 2\int_{1-\delta}^{1} r_D\psi_D \mathrm{d}r_D = \frac{\sqrt{48\beta\eta_{D1}t_D}}{3} \qquad t_D < \frac{1}{48\beta\eta_{D1}}. \tag{A8}$$

[89] Equation (A8) is the same as equation (28) in the main text.

[90] The late time solution of the nonlinear PDE using the method of moments is explained in more details in this part. For the late time solution the following equation is used as the initial condition, which comes from the early time solution:

$$t_D = \frac{1}{48\beta\eta_{D1}} \rightarrow \psi_D = r_D^4. \tag{A9}$$

[91] The inner and outer boundary conditions and the diffusivity equation are the same as equations (26), (27), and (24) (with I=1), respectively. The method of moments is used to find the late time solution of this PDE by suggesting the following trial solution and the residual (R) as follows:

$$\psi_D(r_D,t_D) = A(t_D) + B(t_D)r_D + C(t_D)r_D^2 + D(t_D)r_D^4 \qquad t_D \geq \frac{1}{48\beta\eta_{D1}}, \tag{A10}$$

$$R = r_D\frac{\partial\psi_D}{\partial t_D} - \frac{\partial}{\partial r_D}\left(\beta\eta_D r_D\frac{\partial\psi_D}{\partial r_D}\right). \tag{A11}$$

[92] The unknown coefficients (A, B, C, and D) in equation (A10) are found by using the boundary conditions and making the zero and first moments of R vanish by enforcing the following conditions:

$$\int_0^1 R\mathrm{d}r_D = 0 \rightarrow \int_0^1 \left(r_D\frac{\partial\psi_D}{\partial t_D} - \frac{\partial}{\partial r_D}\left(\beta\eta_D r_D\frac{\partial\psi_D}{\partial r_D}\right)\right)\mathrm{d}r_D = 0, \tag{A12}$$

$$\int_0^1 r_D R\mathrm{d}r_D = 0 \rightarrow \int_0^1 r_D\left[r_D\frac{\partial\psi_D}{\partial t_D} - \frac{\partial}{\partial r_D}\left(\beta\eta_D r_D\frac{\partial\psi_D}{\partial r_D}\right)\right]\mathrm{d}r_D = 0. \tag{A13}$$

[93] From the inner boundary conditions, we can conclude that $B = 0$; the outer boundary condition (equation (27)) leads to:

$$A = 1 - C - D. \tag{A14}$$

[94] Solving equations (A12) and (A13), combining the results with equation (A14) and some simplification lead to a system of ordinary differential equations as follows:

$$\frac{\mathrm{d}C}{\mathrm{d}t_D} = 20\beta\eta_{D1}C + 96\beta\eta_{D1}D, \tag{A15}$$

$$\frac{\mathrm{d}D}{\mathrm{d}t_D} = -21\beta\eta_{D1}C - 84\beta\eta_{D1}D. \tag{A16}$$

[95] Solving the system of the ordinary differential equations leads to the following equations for unknown coefficients C and D:

$$C = -3.725m_1\exp(\omega_1 t_D) - 1.227m_2\exp(\omega_2 t_D), \tag{A17}$$

$$D = m_1\exp(\omega_1 t_D) + m_2\exp(\omega_2 t_D), \tag{A18}$$

[96] where ω_1 and ω_2 are the eigenvalues of the system of the ordinary differential equations and are defined based on equation (30) in the main text. So we have the following equation for the late time dimensionless pseudopressure:

$$\psi_D(r_D,t_D) = (1 + 2.725m_1e^{\omega_1 t_D} + 0.227m_2e^{\omega_2 t_D}) + (-3.725m_1e^{\omega_1 t_D} - 1.227m_2e^{\omega_2 t_D})r_D^2 + (m_1e^{\omega_1 t_D} + m_2e^{\omega_2 t_D})r_D^4, \qquad t_D \geq \frac{1}{48\beta\eta_{D1}}, \tag{A19}$$

where m_1 and m_2 are obtained by using the initial condition of equation (A9), and the trial solution of the nonlinear PDE

for the late time behavior is obtained as in equation (A20). After that, equation (A20) is integrated (equation (A7)) over the matrix block volume to obtain the average matrix block pseudo pressure (equation (29) in the main text).

$$\psi_D(r_D,t_D) = (1 - 1.512e^{\omega_1 t_D} + 1.14e^{\omega_2 t_D}) + (2.067e^{\omega_1 t_D} - 6.162e^{\omega_2 t_D})r_D^2 + (-0.555e^{\omega_1 t_D} + 5.022e^{\omega_2 t_D})r_D^4, \qquad t_D \geq \frac{1}{48\beta\eta_{D1}}. \tag{A20}$$

A2. Variable Fracture Pressure

[97] For the linearly declining fracture pressure, the outer boundary condition (fracture pressure) varies linearly with the time based on the following equation:

$$r = R_m \rightarrow \psi_m = \psi_f = \psi_i(1 - \alpha t) \qquad \alpha \leq \frac{1}{t}. \tag{A21}$$

[98] In this case, the dimensionless pseudopressure and fracture dimensionless pseudopressure are defined as follows:

$$\psi_D = \frac{\psi_i - \psi_m}{\psi_i}, \tag{A22}$$

$$\psi_{fD} = \kappa t_D, \qquad \kappa \leq \frac{1}{t_D}. \tag{A23}$$

[99] For the linearly declining fracture pressure, the diffusivity equation and its initial and inner boundary conditions are the same as equations (24) (with I=1), (25), and (26), respectively. Equation (A23) is used as the outer boundary condition. In this case, the shape factor equation has the following form for a cylindrical block:

$$\sigma R_m^2 = -\frac{1}{\eta_D}\left(\frac{\frac{\partial \bar{\psi}_D}{\partial t_D}}{\bar{\psi}_D - \kappa t_D}\right). \tag{A24}$$

[100] For the early time solution of the linear decline of a cylindrical block we assume that the trial solution has the following form:

$$\psi_D(r_D,t_D) = \kappa t_D\left[1 - \frac{1 - r_D^2}{1 - (1 - \delta(t_D))^2}\right]^2. \tag{A25}$$

[101] In equation (A25), the terms in the bracket is the solution of the constant fracture pressure case. In the case of variable fracture pseudo pressure the penetration depth (numerator in equation (A25)) is found by solving the following ordinary differential equation [*Mitchel and Myers*, 2010; *Ranjbar et al.*, 2011]:

$$\frac{\mathrm{d}}{\mathrm{d}t_D}\left[\frac{\psi_{fD}(t_D)\left\{1 - (1 - \delta(t_D))^2\right\}}{n+1} - \frac{\left\{1 - (1 - \delta(t_D))^2\right\}\theta}{(n+1)^2}\right] = \frac{n\psi_{fD}(t_D) + \theta}{\left\{1 - (1 - \delta(t_D))^2\right\}}. \tag{A26}$$

[102] In this equation, n is the trial solution exponent (n=4 for the cylindrical block) and θ is obtained based on the following equation:

$$\theta = \frac{\frac{\partial \psi_{fD}}{\partial t_D}\left\{1 - (1 - \delta(t_D))^2\right\}^2 - n(n-1)\psi_{fD}}{2n - 1}. \tag{A27}$$

[103] To find a semianalytical solution for the penetration depth we assume that θ=0 in equation (A26) as assumed by *Mitchel and Myers* [2010]. For solving equation (A26), we use the following substitution:

$$1 - (1 - \delta(t_D))^2 = z = \xi\sqrt{t_D}. \tag{A28}$$

[104] Solving equation (A26) for the linear decline leads to the following equation for the penetration depth:

$$\delta(t_D) = 1 - \sqrt{1 - \sqrt{\frac{40\beta\eta_{D1}t_D}{3}}}. \tag{A29}$$

[105] It should be mentioned that a more accurate solution can be obtained if the following equation is used in the trial solution in the case of the linearly declining fracture pressure for the cylindrical matrix block:

$$1 - \delta(t_D) = \sqrt{1 - \sqrt{16\beta\eta_{D1}t_D}}. \tag{A30}$$

[106] In the developed solution, equation (A30) is used for the time-dependent penetration depth. It should be noted that this solution is valid till $1-\delta(t_D)$=0. Substituting the penetration depth equation in the dimensionless pseudo pressure and integrating over the bulk volume of the matrix block leads to the following equations for the early time dimensionless pseudo pressure and the average dimensionless pseudo pressure, respectively:

$$\psi_D = \kappa t_D\frac{\left[r_D^2 - 1 + \sqrt{16\beta\eta_{D1}t_D}\right]^2}{16\beta\eta_{D1}t_D}, \qquad t_D < \frac{1}{16\beta\eta_{D1}}, \tag{A31}$$

$$\bar{\psi}_D = \frac{\kappa t_D\sqrt{16\beta\eta_{D1}t_D}}{3}, \qquad t_D < \frac{1}{16\beta\eta_{D1}}. \tag{A32}$$

[107] Duhamel's theorem is used to find the late time solution of the diffusivity equation when the fracture boundary condition changes with time as follows:

$$\psi_D = \frac{\partial}{\partial t_D}\int_0^{t_D}\psi_{fD}(\tau)\psi_D(r_D, t_D - \tau)\mathrm{d}\tau, \qquad t_D \geq \frac{1}{16\beta\eta_{D1}}. \tag{A33}$$

[108] In this equation, ψ_D within the integral is the solution when $\psi_{fD} = 1$ (equation (A19)) and $\psi_D$on the left-hand side is the solution of the PDE when the matrix-fracture boundary condition changes with time. Substituting equations (A19) and (A23) into Duhamel's equation and using the initial condition (at $t_D = \frac{1}{16\beta\eta_{D1}}$ we have $\psi_D = \frac{\kappa}{16\beta\eta_{D1}}r_D^4$) leads to the following late time solution for the dimensionless pseudopressure for the linearly declining fracture pressure and the cylindrical matrix block:

$$\psi_D(r_D,t_D)=\kappa t_D-\frac{0.58526\kappa}{\omega_1}\left(2.725-3.725r_D^2+r_D^4\right)\left(e^{\omega_1 t_D}-1\right)+\frac{5.57480\kappa}{\omega_2}\left(0.227-1.227r_D^2+r_D^4\right)\left(e^{\omega_2 t_D}-1\right),\quad t_D\geq\frac{1}{16\beta\eta_{D1}}. \tag{A34}$$

[109] Integrating this equation over the bulk volume of the cylindrical matrix block with linearly declining fracture pressure (equation (A7)) leads to the following equation:

$$\overline{\psi}_D=\kappa t_D-\frac{0.69987\kappa}{\omega_1}\left(e^{\omega_1 t_D}-1\right)-\frac{0.29639\kappa}{\omega_2}\left(e^{\omega_2 t_D}-1\right),\quad t_D\geq\frac{1}{16\beta\eta_{D1}}. \tag{A35}$$

[110] For exponentially declining fracture pressure, we have the same PDE with the same initial and inner boundary conditions with the following outer boundary condition:

$$r=R_m\rightarrow\psi_m=\psi_f(t)=\psi_\infty+(\psi_i-\psi_\infty)\exp(-\alpha t). \tag{A36}$$

[111] In this equation, ψ_∞ is the fracture pseudopressure when time tends to the infinity. In this case, the dimensionless pseudopressure and the dimensionless fracture pseudopressure are defined as follows:

$$\psi_D=\frac{\psi_m-\psi_i}{\psi_\infty-\psi_i}, \tag{A37}$$

$$\psi_{fD}=1-\exp(-\kappa t_D). \tag{A38}$$

[112] In this case, the diffusivity equation and its initial and boundary conditions are the same as equations (24) (with I=1), (25), and (26), respectively, with equation (A38) as the outer boundary condition. The dimensionless shape factor equation has the following form for a cylindrical block and exponentially declining fracture pressure:

$$\sigma R_m^2=-\frac{1}{\eta_D}\left(\frac{\frac{\partial\overline{\psi}_D}{\partial t_D}}{\overline{\psi}_D-(1-\exp(-\kappa t_D))}\right). \tag{A39}$$

[113] For the early time solution of the exponential decline we assume that the trial solution has the following form:

$$\psi_D(r_D,t_D)=(1-\exp(-\kappa t_D))\left[1-\frac{1-r_D^2}{1-(1-\delta(t_D))^2}\right]^2. \tag{A40}$$

[114] Using equations (A26) and (A28) and comparison with the literature model [*Hassanzadeh and Pooladi-Darvish*, 2006] leads to the following equation for penetration depth in the case of exponentially declining fracture pressure:

$$1-\delta(t_D)=\sqrt{1-\sqrt{24\beta\eta_{D1}t_D\left(\frac{2}{1-e^{-\kappa t_D}}-\frac{\sqrt{\pi}}{1-e^{-\kappa t_D}}\frac{\operatorname{erf}\left(\sqrt{\kappa t_D}\right)}{\sqrt{\kappa t_D}}\right)}}. \tag{A41}$$

[115] It should be noted that the effect of pressure disturbance will reach the inner boundary when 1-$\delta(t_D)$=0 and for the exponential decline we cannot obtain an explicit equation for t^* and it is determined for any values of k by making equation (A41) equal to zero. Therefore, the early time solution for the exponentially declining fracture pressure and cylindrical matrix block can be expressed as follows:

$$\psi_D(r_D,t_D)=(1-e^{-\kappa t_D})\times\frac{\left[r_D^2-1+\sqrt{24\beta\eta_{D1}t_D\left(\frac{2}{1-e^{-\kappa t_D}}-\frac{\sqrt{\pi}}{1-e^{-\kappa t_D}}\frac{\operatorname{erf}\left(\sqrt{\kappa t_D}\right)}{\sqrt{\kappa t_D}}\right)}\right]^2}{24\beta\eta_{D1}t_D\left(\frac{2}{1-e^{-\kappa t_D}}-\frac{\sqrt{\pi}}{1-e^{-\kappa t_D}}\frac{erf\left(\sqrt{\kappa t_D}\right)}{\sqrt{\kappa t_D}}\right)},\quad t_D<t^*. \tag{A42}$$

[116] The initial condition for the late time solution comes from the early time solution (equation (A42)) as follows:

$$t_D=t^*\rightarrow\psi_D=(1-\exp(-\kappa t^*))r_D^4. \tag{A43}$$

[117] The diffusivity equation and its boundary conditions are the same as before (equations (24), (with I=1), (26), and (27)). Using Duhamel's theorem (equation (A33)) and the solution of the constant fracture pressure (equation (A19)) leads to the following late time solution for the case of the exponentially declining fracture pressure:

$$\psi_D(r_D,t_D)=1-e^{-\kappa t_D}+\left\{2.725m_1\left(1-\frac{\omega_1}{\kappa+\omega_1}\right)e^{\omega_1 t_D}+0.227m_2\left(1-\frac{\omega_2}{\kappa+\omega_2}\right)e^{\omega_2 t_D}-\left(\frac{2.725\kappa m_1}{\kappa+\omega_1}+\frac{0.227\kappa m_2}{\kappa+\omega_2}\right)e^{-\kappa t_D}\right\}-\left\{\overbrace{3.725m_1\left(1-\frac{\omega_1}{\kappa+\omega_1}\right)e^{\omega_1 t_D}+1.227m_2\left(1-\frac{\omega_2}{\kappa+\omega_2}\right)e^{\omega_2 t_D}-\left(\frac{3.725\kappa m_1}{\kappa+\omega_1}+\frac{1.227\kappa m_2}{\kappa+\omega_2}\right)e^{-\kappa t_D}}^{C}\right\}r_D^2+\left\{\overbrace{m_1\left(1-\frac{\omega_1}{\kappa+\omega_1}\right)e^{\omega_1 t_D}+m_2\left(1-\frac{\omega_2}{\kappa+\omega_2}\right)e^{\omega_2 t_D}-\left(\frac{\kappa m_1}{\kappa+\omega_1}+\frac{\kappa m_2}{\kappa+\omega_2}\right)e^{-\kappa t_D}}^{D}\right\}r_D^4,\quad t_D\geq t^*. \tag{A44}$$

[118] The initial condition is used to find m_1 and m_2 as follows:

$$t_D = t^* \rightarrow C = 0, \qquad D = 1 - \exp(-\kappa t^*). \tag{A45}$$

[119] Solving the system of equations (A45) leads to the following values for m_1 and m_2:

$$\begin{cases} m_1 = -0.49119 \dfrac{\kappa + \omega_1}{\kappa} \dfrac{1 - e^{-\kappa t^*}}{e^{\omega_1 t^*} - e^{-\kappa t^*}} \\ m_2 = 1.49118 \dfrac{\kappa + \omega_2}{\kappa} \dfrac{1 - e^{-\kappa t^*}}{e^{\omega_2 t^*} - e^{-\kappa t^*}} \end{cases}. \tag{A46}$$

[120] Using these values in equation (A44) and simplifying lead to the following late time pseudopressure for the exponentially declining fracture pressure:

$$\begin{aligned} \psi_D(r_D, t_D) &= 1 - e^{-\kappa t_D} - 0.49119 \left(\frac{1 - e^{-\kappa t^*}}{e^{\omega_1 t^*} - e^{-\kappa t^*}} \right) \\ &\times e^{\omega_1 t_D} \left(2.725 - 3.725 r_D^2 + r_D^4 \right) \\ &+ 1.49118 \left(\frac{1 - e^{-\kappa t^*}}{e^{\omega_2 t^*} - e^{-\kappa t^*}} \right) e^{\omega_2 t_D} \left(0.227 - 1.227 r_D^2 + r_D^4 \right) \\ &+ \left[\begin{array}{l} 0.49119 \left(\dfrac{1 - e^{-\kappa t^*}}{e^{\omega_1 t^*} - e^{-\kappa t^*}} \right) \left(2.725 - 3.725 r_D^2 + r_D^4 \right) - \\ 1.49118 \left(\dfrac{1 - e^{-\kappa t^*}}{e^{\omega_2 t^*} - e^{-\kappa t^*}} \right) \left(0.227 - 1.227 r_D^2 + r_D^4 \right) \end{array} \right] e^{-\kappa t_D}, \\ & t_D \geq t^*. \end{aligned} \tag{A47}$$

[121] Integrating of the pseudo pressure equations over the bulk volume of the cylindrical matrix block (equation (A7)) leads to the following equations for early and late time average dimensionless pseudopressure when the fracture pressure declines exponentially with time for the cylindrical matrix block:

$$\begin{aligned} \overline{\psi}_D &= \frac{\sqrt{1 - e^{-\kappa t_D}}}{3} \times \sqrt{24 \beta \eta_{D1} t_D \left(2 - \frac{\sqrt{\pi} \operatorname{erf}\left(\sqrt{\kappa t_D} \right)}{\sqrt{\kappa t_D}} \right)}, \\ & t_D < t^*. \end{aligned} \tag{A48}$$

$$\begin{aligned} \overline{\psi}_D = 1 - e^{-\kappa t_D} &- 0.58746 \left(\frac{1 - e^{-\kappa t^*}}{e^{\omega_1 t^*} - e^{-\kappa t^*}} \right) e^{\omega_1 t_D} \\ &- 0.07754 \left(\frac{1 - e^{-\kappa t^*}}{e^{\omega_2 t^*} - e^{-\kappa t^*}} \right) e^{\omega_2 t_D} + \left[0.58746 \left(\frac{1 - e^{-\kappa t^*}}{e^{\omega_1 t^*} - e^{-\kappa t^*}} \right) \right. \\ &\left. + 0.07754 \left(\frac{1 - e^{-\kappa t^*}}{e^{\omega_2 t^*} - e^{-\kappa t^*}} \right) \right] e^{-\kappa t_D}, \qquad t_D \geq t^*. \end{aligned} \tag{A49}$$

A3. Variable Block Size Distributions With Cylindrical Matrix Blocks

[122] In this section the solution of PDE (equation (62), with I=1) with its initial and boundary conditions (equations (63)–(65)) for variable block size distribution is discussed in more details.

[123] The integral method is used to derive the early time approximate solution of the diffusivity equation for flow of compressible and slightly compressible fluids in the cylindrical matrix block for different block size distributions. For the early time solution, in addition to the diffusivity equation (equation (62), with I=1) and outer boundary condition (equation (65)), we have the following condition at the radius where the pressure disturbance has reached:

$$r_D = R_{De} - \delta(t_D) \rightarrow \psi_D = 0, \quad \frac{\partial \psi_D}{\partial r_D} = 0. \tag{A50}$$

[124] Similar to the single matrix block we suggest a fourth-order polynomial trial solution (equation (A3)) to be used in the integral method. Using the actual and auxiliary boundary conditions (equations (65) and (A50)) in the trial solution leads to the following equations for A, B and C coefficients:

$$A = \frac{[R_{De} - \delta]^4}{\left[R_{De}^2 - (R_{De} - \delta)^2 \right]^2}, \tag{A51}$$

$$B = \frac{2[R_{De} - \delta]^2}{\left[R_{De}^2 - (R_{De} - \delta)^2 \right]^2}, \tag{A52}$$

$$C = \frac{1}{\left[R_{De}^2 - (R_{De} - \delta)^2 \right]^2}. \tag{A53}$$

[125] Substituting these equations for time-dependent coefficients and some simplification leads to the following equation:

$$\psi_D = \frac{\left[r_D^2 - (R_{De} - \delta)^2 \right]^2}{\left[R_{De}^2 - (R_{De} - \delta)^2 \right]^2}. \tag{A54}$$

[126] Using this trial solution (equation (A54)) in the integral form of the diffusivity equation (from R_{De}-δ to R_{De}) leads to the following ordinary differential equation (ODE):

$$\frac{1}{6} \frac{\mathrm{d}}{\mathrm{d}t_D} \left[R_{De}^2 - (R_{De} - \delta)^2 \right] = \frac{4 \beta \eta_{D1} R_{De}^2}{R_{De}^2 - (R_{De} - \delta)^2}. \tag{A55}$$

[127] Solving this ODE leads to the following equation for penetration depth and early time pseudo pressure:

$$\delta = R_{De} - \sqrt{R_{De}^2 - R_{De} \sqrt{48 \beta \eta_{D1} t_D}} \quad \text{and} \quad \delta < R_{De}, \tag{A56}$$

$$\psi_D = \frac{\left[r_D^2 - R_{De}^2 + R_{De} \sqrt{48 \beta \eta_{D1} t_D} \right]^2}{48 R_{De}^2 \beta \eta_{D1} t_D} \qquad t_D < \frac{R_{De}^2}{48 \beta \eta_{D1}}. \tag{A57}$$

[128] The early time average dimensionless pseudopressure is obtained by integrating over the bulk volume of the matrix block:

$$\begin{aligned} \overline{\psi}_D &= \frac{2}{R_{De}^2} \int_{R_{De} - \delta}^{R_{De}} r_D \frac{\left[r_D^2 - R_{De}^2 + R_{De} \sqrt{48 \beta \eta_{D1} t_D} \right]^2}{48 R_{De}^2 \beta \eta_{D1} t_D} dr_D \\ &= \frac{\sqrt{48 \beta \eta_{D1} t_D}}{3 R_{De}} \qquad t_D < \frac{R_{De}^2}{48 \beta \eta_{D1}}. \end{aligned} \tag{A58}$$

[129] For the late time solution we have the same PDE (equation (62), with I=1) with the same boundary conditions (equations (64) and (65)) and the following initial condition:

$$t_D = \frac{R_{De}^2}{48\beta\eta_{D1}} \rightarrow \psi_D = \frac{1}{R_{De}^4} r_D^4. \tag{A59}$$

[130] The method of moments is used to find the late time solution of this PDE by suggesting a fourth-order trial solution (equation (A10)) and the residual (R) as equation (A11). The unknown coefficients (A, B, C and D) in equation (A10) are found by using the boundary conditions and making the zero and first moments of R vanish by enforcing the following conditions:

$$\int_0^{R_{De}} R\mathrm{d}r_D = 0 \rightarrow \int_0^{R_{De}} \left(r_D \frac{\partial \psi_D}{\partial t_D} - \frac{\partial}{\partial r_D}\left(\beta\eta_D r_D \frac{\partial \psi_D}{\partial r_D} \right) \right) \mathrm{d}r_D = 0, \tag{A60}$$

$$\int_0^{R_{De}} r_D R\mathrm{d}x_D = 0 \rightarrow \int_0^{R_{De}} r_D \left[r_D \frac{\partial \psi_D}{\partial t_D} - \frac{\partial}{\partial r_D}\left(\beta\eta_D r_D \frac{\partial \psi_D}{\partial r_D} \right) \right] \mathrm{d}r_D = 0. \tag{A61}$$

[131] From the inner boundary conditions, we can conclude that $B = 0$; the outer boundary condition (equation (65)) leads to:

$$A = 1 - CR_{De}^2 - DR_{De}^4. \tag{A62}$$

[132] Solving equations (A60) and (A61), combining the results with equation (A62) and some simplification lead to a system of ODEs as follows:

$$\frac{\mathrm{d}C}{\mathrm{d}t_D} = \frac{20\beta\eta_{D1}}{R_{De}^2} C + 96\beta\eta_{D1} D, \tag{A63}$$

$$\frac{\mathrm{d}D}{\mathrm{d}t_D} = \frac{-21\beta\eta_{D1}}{R_{De}^4} C - \frac{84\beta\eta_{D1}}{R_{De}^2} D. \tag{A64}$$

[133] Solving the system of ordinary differential equations leads to the following equations for the unknown coefficients C and D:

$$C = -3.725R_{De}^2 m_1 \exp(\omega_1 t_D) - 1.227R_{De}^2 m_2 \exp(\omega_2 t_D), \tag{A65}$$

$$D = m_1 \exp(\omega_1 t_D) + m_2 \exp(\omega_2 t_D), \tag{A66}$$

[134] where ω_1 and ω_2 are the eigenvalues of the system of the ordinary differential equation and are defined based on equation (71) in the main text.

[135] The initial condition (equation (A59)) is used to find m_1 and m_2. Therefore, m_1 and m_2 are found by solving the following system of equations:

$$\begin{aligned} &-3.725R_{De}^2 m_1 \exp\left(\omega_1 \frac{R_{De}^2}{48\beta\eta_{D1}} \right) \\ &- 1.227R_{De}^2 m_2 \exp\left(\omega_2 \frac{R_{De}^2}{48\beta\eta_{D1}} \right) = 0, \end{aligned} \tag{A67}$$

$$m_1 \exp\left(\omega_1 \frac{R_{De}^2}{48\beta\eta_{D1}} \right) + m_2 \exp\left(\omega_2 \frac{R_{De}^2}{48\beta\eta_{D1}} \right) = \frac{1}{R_{De}^4}. \tag{A68}$$

[136] Solving this system of equations for m_1 and m_2 and substituting in the time-dependent coefficients of the trial solution, the late time behavior is obtained as follows:

$$\begin{aligned} \psi_D(r_D, t_D) = {} & (1 - 1.512e^{\omega_1 t_D} + 1.14e^{\omega_2 t_D}) \\ & + \left(\frac{2.067}{R_{De}^2} e^{\omega_1 t_D} - \frac{6.162}{R_{De}^2} e^{\omega_2 t_D} \right) r_D^2 \\ & + \left(\frac{-0.555}{R_{De}^4} e^{\omega_1 t_D} + \frac{5.022}{R_{De}^4} e^{\omega_2 t_D} \right) r_D^4, \quad t_D \geq \frac{R_{De}^2}{48\beta\eta_{D1}}. \end{aligned} \tag{A69}$$

[137] After that, equations (A69) is integrated over the matrix block volume to obtain the late time average matrix block pseudo-pressure as follows:

$$\begin{aligned} \overline{\psi}_D = \frac{2}{R_{De}^2} \int_0^{R_{De}} r_D \psi_D \mathrm{d}r_D = 1 - 0.664e^{\omega_1 t_D} - 0.267e^{\omega_2 t_D} \\ t_D \geq \frac{R_{De}^2}{48\beta\eta_{D1}} \end{aligned} . \tag{A70}$$

Appendix B: Analytical Solution for Spherical Blocks

[138] In this appendix, the solution of nonlinear gas pressure diffusion in a spherical matrix block is discussed in more details.

B1. Constant Fracture Pressure

[139] In this section, the solution of PDE (equation (24), with I=2) with the initial and boundary conditions (equations (25)–(27)) is presented.

[140] The integral method [*Zimmerman and Bodvarsson*, 1989] is used to find the early time solution of this equation by defining the time-dependent penetration depth, $\delta(t_D)$, in which the pressure disturbance has reached. For the early time solution, in addition to the outer boundary condition (equation (27)), we have the following auxiliary boundary conditions:

$$r_D = 1 - \delta(t_D) = \varepsilon(t_D) \rightarrow \psi_D = 0, \quad \frac{\partial \psi_D}{\partial r_D} = 0, \quad \frac{\partial^2 \psi_D}{\partial r_D^2} = 0. \tag{B1}$$

[141] The following third-order polynomial trial solution is suggested to be used in the integral method:

$$\psi_D = A(t_D) + B(t_D) r_D + C(t_D) r_D^2 + D(t_D) r_D^3. \tag{B2}$$

[142] Using the actual and auxiliary boundary conditions in the trial solution leads to the following equation for dimensionless pseudopressure:

$$\psi_D = \frac{(r_D - \varepsilon)^3}{(1 - \varepsilon)^3}. \tag{B3}$$

[143] Using this trial solution in the integral form of the diffusivity equation (equation (24), with I=2) leads to the following ODE:

$$\frac{3\beta\eta_{D1}}{1-\varepsilon}=\frac{\mathrm{d}}{\mathrm{d}t_D}\left[\frac{\varepsilon^6-20\varepsilon^3+45\varepsilon^2-36\varepsilon+10}{60(1-\varepsilon)^3}\right]\rightarrow \quad 180\beta\eta_{D1}\mathrm{d}t_D=(\varepsilon-1)\mathrm{d}\left[\varepsilon^3+3\varepsilon^2+6\varepsilon-10\right]. \tag{B4}$$

[144] Solving this ODE leads to the following equation:

$$t_D=\frac{3\varepsilon^4+4\varepsilon^3-24\varepsilon+17}{720\beta\eta_{D1}}. \tag{B5}$$

[145] This solution is valid till $\varepsilon=0$ or $t_D<\frac{17}{720\beta\eta_{D1}}$.

[146] Equation (B3) is integrated over the bulk volume of the matrix block to determine the average dimensionless pseudopressure as follows:

$$\overline{\psi}_D=3\int_{\varepsilon}^{1}r_D^2\psi_D\mathrm{d}r_D=3\int_{\varepsilon}^{1}r_D^2\frac{(r_D-\varepsilon)^3}{(1-\varepsilon)^3}\mathrm{d}r_D=-\frac{\varepsilon^3+3\varepsilon^2+6\varepsilon-10}{20}, \quad t_D<\frac{17}{720\beta\eta_{D1}} \tag{B6}$$

[147] Equations (B5) and (B6) in terms of penetration depth δ can be expressed as follows:

$$\overline{\psi}_D=\frac{\delta^3-6\delta^2+15\delta}{20}, \qquad t_D<\frac{17}{720\beta\eta_{D1}}, \tag{B7}$$

$$t_D=\frac{3\delta^4-16\delta^3+30\delta^2}{720\beta\eta_{D1}}. \tag{B8}$$

[148] For the late time solution we have the following initial condition (the diffusivity equation and boundary conditions are the same as equations (24), (26), and (27), respectively):

$$t_D=\frac{17}{720\beta\eta_{D1}}\rightarrow\psi_D=r_D^3. \tag{B9}$$

[149] The method of moments is used to find the late time solution of this PDE by suggesting a third-order trial solution as equation (B2) and the residual (R) as follows:

$$R=\frac{\partial}{\partial r_D}\left(\beta\eta_D(t_D)r_D^2\frac{\partial\psi_D}{\partial r_D}\right)-r_D^2\frac{\partial\psi_D}{\partial t_D}. \tag{B10}$$

[150] The unknown coefficients (A, B, C, and D) in equation (B2) are found using the boundary conditions and making the zero and first moments of R vanish by enforcing the following conditions:

$$\int_0^1 R\mathrm{d}r_D=0\rightarrow\int_0^1\left(r_D^2\frac{\partial\psi_D}{\partial t_D}-\frac{\partial}{\partial r_D}\left(\beta\eta_D r_D^2\frac{\partial\psi_D}{\partial r_D}\right)\right)\mathrm{d}r_D=0, \tag{B11}$$

$$\int_0^1 r_D R\mathrm{d}r_D=0\rightarrow\int_0^1 r_D\left[r_D^2\frac{\partial\psi_D}{\partial t_D}-\frac{\partial}{\partial r_D}\left(\beta\eta_D r_D^2\frac{\partial\psi_D}{\partial r_D}\right)\right]\mathrm{d}r_D=0. \tag{B12}$$

[151] From the first boundary conditions, we can conclude that $B=0$; the second boundary condition (equation (27)) leads to:

$$A=1-C-D. \tag{B13}$$

[152] Solving equations (B11) and (B12), combining the results with equation (B13) and some simplification leads to a system of ODEs as follows:

$$\frac{\mathrm{d}C}{\mathrm{d}t_D}=90\beta\eta_{D1}C+198\beta\eta_{D1}D, \tag{B14}$$

$$\frac{\mathrm{d}D}{\mathrm{d}t_D}=-84\beta\eta_{D1}C-176.4\beta\eta_{D1}D. \tag{B15}$$

[153] Solving the system of ordinary differential equations leads to the following equations for unknown coefficients C and D:

$$C=-1.982384m_1\exp(\omega_1 t_D)-1.189044m_2\exp(\omega_2 t_D), \tag{B16}$$

$$D=m_1\exp(\omega_1 t_D)+m_2\exp(\omega_2 t_D), \tag{B17}$$

[154] where ω_1 and ω_2 are the eigenvalues of the system of ODEs and are defined based on equation (34) in the main text. So we have the following equation for the late time dimensionless pseudopressure:

$$\psi_D=1+0.982384m_1e^{\omega_1 t_D}+0.189044m_2e^{\omega_2 t_D}+(-1.982384m_1e^{\omega_1 t_D}-1.189044m_2e^{\omega_2 t_D})r_D^2+(m_1e^{\omega_1 t_D}+m_2e^{\omega_2 t_D})r_D^3, \qquad t_D\geq\frac{17}{720\beta\eta_{D1}}. \tag{B18}$$

[155] The initial condition of equation (B9) is used to find m_1 and m_2. Therefore, the trial solution of the nonlinear PDE for the late time behavior is obtained as follows:

$$\psi_D=1-1.859229e^{\omega_1 t_D}+2.877049e^{\omega_2 t_D}+(3.751798e^{\omega_1 t_D}-18.095987e^{\omega_2 t_D})r_D^2+(-1.892569e^{\omega_1 t_D}+15.218938e^{\omega_2 t_D})r_D^3, \quad t_D\geq\frac{17}{720\beta\eta_{D1}}. \tag{B19}$$

[156] After that, equations (B19) is integrated (equation (B6)) over the matrix block volume to obtain the average matrix block pseudopressure as follows:

$$\overline{\psi}_D=1-0.554435e^{\omega_1 t_D}-0.371074e^{\omega_2 t_D}, \qquad t_D\geq\frac{17}{720\beta\eta_{D1}}. \tag{B20}$$

B2. Variable Fracture Pressure

[157] In the case of linear decline for the spherical block the outer boundary condition is given in equation (A23).

The PDE and initial and inner boundary conditions are the same as equations (24) (with I=2), (25), and (26), respectively. For the early time solution of the linear decline, we assume that the trial solution has the following form:

$$\psi_D = \kappa t_D \frac{(r_D-\varepsilon)^3}{(1-\varepsilon)^3} = \kappa t_D \left(\frac{r_D+\delta-1}{\delta}\right)^3. \tag{B21}$$

[158] In the case of variable fracture pseudopressure, the penetration depth is found by solving the following ODE [*Mitchel and Myers*, 2010; *Ranjbar et al*., 2011]:

$$\frac{\mathrm{d}}{\mathrm{d}t_D}\left[\frac{\psi_{fD}(t_D)\delta(t_D)}{n+1} - \frac{\delta(t_D)\theta}{(n+1)^2}\right] = \frac{n\psi_{fD}(t_D)+\theta}{\delta(t_D)}. \tag{B22}$$

[159] Using the same procedure as described in section A.2 for the cylindrical block and comparing with the literature model leads to the following equation for early time dimensionless pseudopressure:

$$\psi_D = \kappa t_D \left(\frac{r_D+\sqrt{13\beta\eta_{D1}t_D}-1}{\sqrt{13\beta\eta_{D1}t_D}}\right)^3 \qquad t_D < \frac{1}{13\beta\eta_{D1}}. \tag{B23}$$

[160] Integrating over the bulk volume of the matrix block leads to the following equation for early time average dimensionless pseudopressure:

$$\overline{\psi}_D = \frac{\kappa}{260\beta\eta_{D1}}\left(\delta^5 - 6\delta^4 + 15\delta^3\right) \qquad t_D < \frac{1}{13\beta\eta_{D1}} \text{ or } \delta < 1. \tag{B24}$$

[161] Duhamel's theorem (equation (A33)) is used to find the late time solution of the diffusivity equation in fractured media when the fracture boundary condition changes with time. Substituting equations (B18) and (A23) in Duhamel's equation and using the initial condition (at $t_D = \frac{1}{13\beta\eta_{D1}}$ we have $\psi_D = \frac{\kappa}{13\beta\eta_{D1}} r_D^3$) leads to the following late time solution for dimensionless pseudopressure for the linearly declining fracture pressure and spherical matrix block:

$$\begin{aligned}\psi_D = {} & \kappa t_D - \frac{2.102174\kappa(e^{\omega_1 t_D}-1)}{\omega_1} + \frac{2.788337\kappa(e^{\omega_2 t_D}-1)}{\omega_2} + \\ & \left(\frac{4.241990\kappa(e^{\omega_1 t_D}-1)}{\omega_1} - \frac{17.538009\kappa(e^{\omega_2 t_D}-1)}{\omega_2}\right) r_D^2 + \\ & \left(\frac{-2.139843\kappa(e^{\omega_1 t_D}-1)}{\omega_1} + \frac{14.749672\kappa(e^{\omega_2 t_D}-1)}{\omega_2}\right) r_D^3 \\ & t_D \geq \frac{1}{13\beta\eta_{D1}}.\end{aligned} \tag{B25}$$

[162] Integration of this equation over the bulk volume of the matrix block (equation (B6)) from zero to one leads to the following equation for the average dimensionless pseudopressure of a spherical block when the fracture pressure declines linearly with time:

$$\begin{aligned}\overline{\psi}_D = {} & \kappa t_D - \frac{0.626902\kappa}{\omega_1}(e^{\omega_1 t_D}-1) - \frac{0.359632\kappa}{\omega_2}(e^{\omega_2 t_D}-1), \\ & t_D \geq \frac{1}{13\beta\eta_{D1}}.\end{aligned} \tag{B26}$$

[163] For exponentially declining fracture pressure, the same approach is used and the following equations are obtained for early and late time dimensionless pseudopressure:

$$\begin{aligned}\psi_D(r_D,t_D) = {} & (1-e^{-\kappa t_D}) \\ & \times \left[\frac{r_D - 1 + \sqrt{18\beta\eta_{D1}t_D\left(\frac{2}{1-e^{-\kappa t_D}} - \frac{\sqrt{\pi}}{1-e^{-\kappa t_D}}\frac{\mathrm{erf}\left(\sqrt{\kappa t_D}\right)}{\sqrt{\kappa t_D}}\right)}}{\sqrt{18\beta\eta_{D1}t_D\left(\frac{2}{1-e^{-\kappa t_D}} - \frac{\sqrt{\pi}}{1-e^{-\kappa t_D}}\frac{\mathrm{erf}\left(\sqrt{\kappa t_D}\right)}{\sqrt{\kappa t_D}}\right)}}\right]^3, \\ & t_D < t^*,\end{aligned} \tag{B27}$$

$$\begin{aligned}\psi_D(r_D,t_D) = {} & 1 - e^{-\kappa t_D} + 1.498783\left(\frac{1-e^{-\kappa t^*}}{e^{-\kappa t^*} - e^{\omega_1 t^*}}\right) \\ & e^{\omega_1 t_D}\left(0.982384 - 1.982384 r_D^2 + r_D^3\right) - 2.498783\left(\frac{1-e^{-\kappa t^*}}{e^{-\kappa t^*} - e^{\omega_2 t^*}}\right) \\ & e^{\omega_2 t_D}\left(0.189044 - 1.189044 r_D^2 + r_D^3\right) \qquad t_D \geq t^* \\ & - \begin{bmatrix} 1.498783\left(\frac{1-e^{-\kappa t^*}}{e^{-\kappa t^*} - e^{\omega_1 t^*}}\right)\left(0.982384 - 1.982384 r_D^2 + r_D^3\right) - \\ 2.498783\left(\frac{1-e^{-\kappa t^*}}{e^{-\kappa t^*} - e^{\omega_2 t^*}}\right)\left(0.189044 - 1.189044 r_D^2 + r_D^3\right) \end{bmatrix} e^{-\kappa t_D}.\end{aligned} \tag{B28}$$

B3. Variable Block Size Distributions With Spherical Matrix Blocks

[164] In the case of multiple spherical blocks with variable block size distribution, the diffusivity equation (equation (62), with I=2) with the initial and boundary conditions (equations (63)–(65)) should be solved. The integral method is used to find the early time solution with the following auxiliary equation:

$$r_D = R_{De} - \delta(t_D) = \varepsilon(t_D) \rightarrow \psi_D = 0, \quad \frac{\partial \psi_D}{\partial r_D} = 0, \quad \frac{\partial^2 \psi_D}{\partial r_D^2} = 0. \tag{B29}$$

[165] The third-order trial solution as equation (B2) is suggested to be used in the integral method. Using the actual and auxiliary boundary conditions in the trial solution leads to the following equations for dimensionless pseudo-pressure:

$$\psi_D = \frac{[r_D-\varepsilon]^3}{[R_{De}-\varepsilon]^3} = \left[\frac{r_D+\delta-R_{De}}{\delta}\right]^3. \tag{B30}$$

[166] Using this trial solution (equation (B30)) in the integral form of equation (62), with I=2 (From ε to R_{De}) and some simplification leads to the following ODE:

$$\frac{\mathrm{d}}{\mathrm{d}t_D}\left[\frac{-\varepsilon^3 - 3R_{De}\varepsilon^2 - 6R_{De}^2\varepsilon + 10R_{De}^3}{60}\right] = \frac{3\beta\eta_{D1}R_{De}^2}{(R_{De}-\varepsilon)}. \tag{B31}$$

[167] Solving this ODE leads to the following equation:

$$t_D = \frac{3\varepsilon^4 + 4R_{De}\varepsilon^3 - 24R_{De}^3\varepsilon + 17R_{De}^4}{720\beta\eta_{D1}R_{De}^2}. \tag{B32}$$

[168] This equation in terms of penetration depth can be expressed as follows:

$$t_D = \frac{3\delta^4 - 16R_{De}\delta^3 + 30R_{De}^2\delta^2}{720\beta\eta_{D1}R_{De}^2}. \tag{B33}$$

[169] The early time solution is valid till $\delta < R_{De}$ or $t_D < \frac{17R_{De}^2}{720\beta\eta_{D1}}$.

[170] The early time average dimensionless pseudopressure is obtained by integrating over the bulk volume of the matrix block:

$$\overline{\psi}_D = \frac{3}{R_{De}^3}\int_{\varepsilon}^{R_{De}} r_D^2\left[\frac{r_D + \delta - R_{De}}{\delta}\right]^3 \mathrm{d}r_D = \frac{\delta^3 - 6R_{De}\delta^2 + 15R_{De}^2\delta}{20R_{De}^3} \quad t_D < \frac{17R_{De}^2}{720\beta\eta_{D1}}, \tag{B34}$$

where equation (B33) is used to relate the penetration depth to the dimensionless time.

[171] For the late time solution we have the following initial condition and the inner and outer boundary conditions are the same as equations (64) and (65):

$$t_D = \frac{17R_{De}^2}{720\beta\eta_{D1}} \rightarrow \psi_D = \frac{1}{R_{De}^3}r_D^3. \tag{B35}$$

[172] The method of moments is used to find the late time solution of this PDE by suggesting a third-order trial solution (equation (B2)) and the residual (R) as Equation (B10). The unknown coefficients (A, B, C, and D) in the trial solution of Equation (B2) are found by using the boundary conditions and making the zero and first moments of R vanish by enforcing the following conditions:

$$\int_0^{R_{De}} R\mathrm{d}r_D = 0 \rightarrow \int_0^{R_{De}} \left(r_D^2\frac{\partial\psi_D}{\partial t_D} - \frac{\partial}{\partial r_D}\left(\beta\eta_D r_D^2\frac{\partial\psi_D}{\partial r_D}\right)\right)\mathrm{d}r_D = 0, \tag{B36}$$

$$\int_0^{R_{De}} r_D R\mathrm{d}r_D = 0 \rightarrow \int_0^{R_{De}} r_D\left[r_D^2\frac{\partial\psi_D}{\partial t_D} - \frac{\partial}{\partial r_D}\left(\beta\eta_D r_D^2\frac{\partial\psi_D}{\partial r_D}\right)\right]\mathrm{d}r_D = 0. \tag{B37}$$

[173] From the first boundary conditions, we can conclude that $B = 0$; the second boundary condition (equation (65)) leads to:

$$A = 1 - CR_{De}^2 - DR_{De}^4. \tag{B38}$$

[174] Solving equations (B36) and (B37), combining the results with equation (B38) and some simplification leads to a system of ODEs as follows:

$$\frac{\mathrm{d}C}{\mathrm{d}t_D} = \frac{90\beta\eta_{D1}}{R_{De}^2}C + \frac{198\beta\eta_{D1}}{R_{De}}D, \tag{B39}$$

$$\frac{\mathrm{d}D}{\mathrm{d}t_D} = \frac{-84\beta\eta_{D1}}{R_{De}^3}C - \frac{176.4\beta\eta_{D1}}{R_{De}^2}D. \tag{B40}$$

[175] Solving the system of ODEs and using the initial condition for the late time solution (equation (B35)) leads to the following equation for late time pseudo-pressure for multiple spherical blocks:

$$\psi_D = 1 - 1.859229e^{\omega_1 t_D} + 2.877049e^{\omega_2 t_D} + \left(\frac{3.751798}{R_{De}^2}e^{\omega_1 t_D} - \frac{18.095987}{R_{De}^2}e^{\omega_2 t_D}\right)r_D^2 + \left(\frac{-1.892569}{R_{De}^3}e^{\omega_1 t_D} + \frac{15.218938}{R_{De}^3}e^{\omega_2 t_D}\right)r_D^3, \quad t_D \geq \frac{17R_{De}^2}{720\beta\eta_{D1}}, \tag{B41}$$

where ω_1 and ω_2 are defined based on equation (74) in the main text. After that, equation (B41) is integrated over the matrix block volume (from zero to one) to obtain the late time average matrix block pseudopressure as equation (73) in the main text.

Notations

a	Dimensionless exponential distribution constant
A	Cross-sectional area (L^2)
$A(t_D)$	First coefficient of the trial solution
b	Intercept for linear matrix block size distribution
$B(t_D)$	Second coefficient of the trial solution
$C(t_D)$	Third coefficient of the trial solution
c_m	Matrix compressibility (LT^2/M)
$D(t_D)$	Fourth coefficient of the trial solution
$f_i(R_{mi})$	Fraction of the block volume of size R_{mi}
$f(R_m)$	Probability density function
$f_D(R_D)$	Dimensionless probability density function
F_h	Ratio of minimum block size to the maximum block radius
h_m=$2L_c$	Matrix block thickness (L)
k_m	Matrix permeability (L^2)
M	Mean of the distribution
m	Slope of linear matrix block size distribution
N	Number of matrix block sizes
N_t	Total number of matrix blocks
p	pressure (M/LT^2)
q	Matrix-fracture fluid release (L^3/T)
Q	Cumulative fluid release (L^3)
Q_{Dt}	Dimensionless ultimate cumulative release
R_m	Matrix block radius (L)
R_{me}	Equivalent matrix block radius (L)
R	Residual in the method of moments
S	Heat conduction shape factor (L)
t	Time (T)
t^*	Time which the effect of pressure reaches to the inner matrix boundary
T	Reservoir temperature (K)
V_b	Matrix block volume (L^3)
r_D	Dimensionless radius

Greek Symbols

α Radius of cylinder, sphere or half thickness of slab (L)
β Correction factor
δ Penetration depth
ε Un-penetrated depth for spherical block
η Matrix hydraulic diffusivity (L^2/T)
$\overline{\eta}$ Average hydraulic diffusivity (L^2/T)
η_{D1} Dimensionless fracture hydraulic diffusivity
κ Dimensionless exponent and slope in fracture depletion regimes
μ Fluid viscosity (M/LT)
σ Diffusion shape factor ($1/L^2$)
σ^2 Variance of the distribution
τ Dimensionless scale time
φ Porosity
χ Ratio of reservoir radius to the maximum block radius
ψ pseudo-pressure (M/LT^3)
ω Dimensionless exponent of solution of gas diffusivity equation using the moment method

Subscripts

D Dimensionless
e Equivalent
f Fracture
g Gas
i Initial condition
ln Log-normal
m Matrix
min Minimum
max Maximum
R Reservoir
sc Standard conditions

[176] **Acknowledgments.** Financial support of NSERC/AERI (AIEES)/Foundation CMG and iCORE (AITF) Chairs Funds and the Department of Chemical and Petroleum Engineering at the University of Calgary is acknowledged.

References

Altevogt, A. S., and M. A. Celia (2004), Numerical modeling of carbon dioxide in unsaturated soils due to deep subsurface leakage, *Water Resour. Res.*, *40*, W03509, doi:10.1029/2003WR002848.

Ames, W. F. (1965), *Nonlinear Partial Differential Equation in Engineering*, Academic, New York.

Barker, J. A. (1985), Block-geometry functions characterizing transport in densely fissured media, *J. Hydrol.*, *77*, 263–279.

Berger, D., and C. Braester (2000), Gas-water displacement through fracture networks, *Water Resour. Res.*, *36*(11), 3205–3210.

Bogdanov, I. I., Mourzenko, V. V. Thovert, J.-F., and P. M. Adler (2003), Pressure drawdown well tests in fractured porous media, *Water Resour. Res.*, *39*(1), 1021, doi:10.1029/2000WR000080.

Chen, C., and D. Zhang (2010), Pore-scale simulation of density-driven convection in fractured porous media during geological CO_2 sequestration, *Water Resour. Res.*, *46*, W11527, doi:10.1029/2010WR009453.

Civan, F., and M. L. Rasmussen (2002), Analytical hindered-matrix-fracture transfer models for naturally fractured petroleum reservoirs, *paper SPE* 74364, SPE International Petroleum Conference and Exhibition in Mexico, Villahermosa, Mexico.

Falta, R. W. (1995), Analytical solutions for gas flow due to gas injection and extraction from horizontal wells, *Ground Water*, *33*(2), 235–246.

Fan, S. S. T., and Y. C. Yen (1968), Nonsteady compressible flow through anisotropic porous mediums with particular reference to snow, *Water Resour. Res.*, *4*(3), 597–606.

Fitzgerald, S. D., and A. W. Woods (1998), Instabilities during liquid migration into superheated geothermal reservoirs, *Water Resour. Res.*, *34*(9), 2089–2101.

Gerke, H. H., and M. Th. van Genuchten (1993), A dual-porosity model for simulating the preferential movement of water and solutes in structured porous media, *Water Resour. Res.*, *29*(2), 305–319.

Goodman, T. R. (1964), Application of integral methods to transient nonlinear heat transfer, in Advances in Heat Transfer, Editors: Hartnett, J.P. and Irvine, T.F, Jr., pp. 51-122, Academic, New York.

Gwo, J. P., R. O'Brien, and P. M. Jardin (1998), Mass transfer in structured porous media: embedding mesoscale structure and microscale hydrodynamics in a two-region model, *J. Hydrol.*, *208*, 204–222.

Hassanzadeh, H., and M. Pooladi-Darvish (2006), Effect of fracture boundary conditions on matrix-fracture transfer shape factor, *Transp. Porous Media*, *64*, 51–71.

Hassanzadeh, H., M. Pooladi-Darvish, and S. Atabay (2009), Shape factor in the drawdown solution for well testing of dual-porosity systems, *Adv. Water Res.*, *32*(11), 1652–1663.

Holman, J. P. (2010), *Heat Transfer*, 10th ed., McGraw-Hill, Boston.

Hoteit, H., and A. Firoozabadi (2005), Multicomponent fluid flow by discontinuous Galerkin and mixed methods in unfractured and fractured media, *Water Resour. Res.*, *41*, W11412, doi:10.1029/2005WR004339.

Huang, K., Y. W. Tsang, and G. S. Bodvarsson (1999), Simultaneous inversion of air-injection tests in fractured unsaturated tuff at Yucca Mountain, *Water Resour. Res.*, *35*(8), 2375–2386.

Illman, W. A. (2005), Type curve analyses of pneumatic single-hole tests in unsaturated fractured tuff: Direct evidence for a porosity scale effect, *Water Resour. Res.*, *41*, W04018, doi:10.1029/2004WR003703.

Illman, W. A., and S. P. Neuman (2001), Type curve interpretation of a cross-hole pneumatic injection test in unsaturated fractured tuff, *Water Resour. Res.*, *37*(3), 583–603.

Kazemi, H., L. S. Merrill, K. L. Porterfield, and P. R. Zeman (1976), Numerical simulation of water-oil flow in naturally fractured reservoirs, Soc. *Pet. Eng. J.*, 317–326.

Lim, K. T., and K. Aziz (1995), Matrix-fracture transfer shape factors for dual-porosity simulators, *J. Pet. Sci. Eng.*, *13*, 169–178.

Lu, M., and L. D. Connel (2007), A dual-porosity model for gas reservoir flow incorporating adsorption behavior-part I. Theoretical development and asymptotic analysis, Transp. *Porous Media*, *68*,153–173.

McWhorter, D. B. (1990), Unsteady radial flow of gas in the vadose zone, *J. Contam. Hydrol.*, *5*, 297–314.

Mitchel, S. L., and T. G. Myers (2010), Improving the accuracy of heat balance integral methods applied to thermal problems with time dependent boundary conditions, *Int. J. Heat Mass Transfer*, *53*, 3540–3551.

Mora, C. A., and R. A. Wattenbarger (2009), Analysis and verification of dual porosity and CBM shape factors, J. *Can. Pet. Technol. 48*(2), 17–21.

Mourzenko, V. V., I. I. Bogdanov, J. F. Thovert, and P. M. Adler (2011), Three-dimensional numerical simulation of single-phase transient compressible flows and well-tests in fractured formations, *Math. Comput. Simul.*, *81*, 2270–2281.

Novakowski, K. S., and P. A. Lapcevic (1994), Field measurement of radial solute transport in fractured rock, *Water Resour. Res.*, *30*(1), 37–44.

Nuske, P., B. Faigle, R. Helmig, J. Niessner, and I. Neuweiler (2010), Modeling gas-water processes in fractures with fracture flow properties obtained through upscaling, *Water Resour. Res.*, *46*, W09538, doi:10.1029/2009WR008076.

Parker, L., R. Yarwood, and J. Selker (2006), Observations of gas flow in porous media using a light transmission technique, *Water Resour. Res.*, *42*, W05501, doi:10.1029/2005WR004080.

Penuela, G., F. Civan, R. G. Hughes, and M. L. Wiggins (2002), Time-dependent shape factors for interporosity flow in naturally fractured gas-condensate reservoirs, *paper SPE* 75524, SPE Gas Technology Symposium, Calgary, Alberta, Canada.

Pooladi-Darvish, M., W. S. Torkite, and S. M. F. Ali (1994), Steam heating of fractured formations containing heavy oil: basic premises and a single-block analytical model, *paper SPE* 28642, SPE Annual Technical Conference and Exhibition, New Orleans, Louisiana.

Pruess, K. (1983), Heat transfer in fractured geothermal reservoirs with boiling, *Water Resour. Res.*, *19*(1), 201–208.

Ranjbar, E., and H. Hassanzadeh (2011), Matrix-fracture transfer shape factor for modeling flow of a compressible fluid in dual-porosity media, *Adv. Water Res.*, *34*(5), 627–639, doi:10.1016/j.adwatres.2011.02.012.

Ranjbar, E., H. Hassanzadeh, and Z. Chen (2011), Effect of fracture pressure depletion regimes on the dual-porosity shape factor for flow of

compressible fluids in fractured porous media, *Adv. Water Res.*, *34*(12), 1681–1693, doi:10.1016/j.adwatres.2011.09.010.

Ranjbar, E., H. Hassanzadeh, and Z. Chen (2012), One-dimensional matrix-fracture transfer in dual porosity systems with variable block size distribution, *Transp. Porous Media*, *95*(1), 185–212, doi:10.1007/s11242-012-0039-4.

Schrauf, T. W., and D. D. Evans (1986), Laboratory studies of gas flow through a single natural fracture, *Water Resour. Res.*, *22*(7), 1038–1050.

Shan, C. (1995), Analytical solutions for determining vertical air permeability in unsaturated soils, *Water Resour. Res.*, *31*(9), 2193–2200.

Shan, C. (2006), An analytical solutions for transient gas flow in a multiwell system, *Water Resour. Res.*, *42*, W10401, doi:10.1029/2005WR004737.

Shan, C., I. Javandel, and P. A. Whiterspoon (1999), Characterization of leaky faults: Study of air flow in faulted vadose zones, *Water Resour. Res.*, *35*(7), 2007–2013.

Tartakovsky, D. M., S. P. Neuman, and Z. Lu (1999), Conditional stochastic averaging of steady state unsaturated flow by means of Kirchhoff transformation, *Water Resour. Res.*, *35*(3), 731–745, doi:10.1029/1998WR900092.

Thunvik, R., and C. Braester (1990), Gas migration in discrete fracture networks, *Water Resour. Res.*, *26*(10), 2425–2434.

van Genuchten, M. Th., and F. N. Dalton (1986), Models for simulating salt movement in aggregated field soils, *Geodrama*, *38*, 165–183.

van Heel, A. P. G., J. J. van Drop, and P. M. Boerrigter (2008), Heavy oil recovery by steam injection in fractured reservoirs, *paper SPE* 113461, SPE/DOE Symposium on Improved Oil Recovery, Tulsa, Oklahoma, USA.

Wang, Y., and M. B. Dusseault (1991), The effect of quadratic gradient terms on the borehole solution in poroelastic media, *Water Resour. Res.*, *27*(12), 3215–3223.

Warren, J. E., and P. J. Root (1963), The behavior of naturally fractured reservoirs, *Soc. Pet. Eng. J.*, Sept., 245–255.

Wuthicharn, K., and R. W. Zimmerman (2011), Shape factors for irregularly matrix blocks, *paper SPE* 148060, SPE Reservoir Characterization and Simulation Conference and Exhibition, Abu Dhabi, UAE.

Ye, P., and L. F. Ayala (2012), A density-diffusivity approach for the unsteady state analysis of natural gas reservoirs, *J. Nat. Gas Sci. Eng.*, *7*, 22–34.

You, K., H. Zhan, and J. Li (2011), Analysis of models for induced gas flow in the unsaturated zone, *Water Resour. Res.*, *47*, W04515, doi:10.1029/2010WR009985.

Zimmerman, R. W., and G. S. Bodvarsson (1989), Integral method solution for diffusion into a spherical block, *J. Hydrol.*, *111*, 213–224.

Zimmerman, R. W., and G. S. Bodvarsson (1995), Effective block size for imbibitions or absorption in dual-porosity media, *Geophys. Res. Lett.*, *22*(11), 1461–1464.

Zimmerman, R. W., G. S. Bodvarsson, and E. M. Kwicklis (1990), Absorption of water into porous blocks of various shapes and sizes, *Water Resour. Res.*, *26*(11), 2797–2806.

Zimmerman, R. W., G. Chen, T. Hadgu, and G. S. Bodvarsson (1993) A numerical dual-porosity model with semi-analytical treatment of fracture/matrix flow, *Water Resour. Res.*, *29*(7), 2127–2137.

Zimmerman, R. W., T. Hadgu, and G. S. Bodvarsson (1996), A new lumped-parameter model for flow in unsaturated dual-porosity media, *Adv. Water Res.*, *19*(5), 317–327.